DEHUMIDIFICATION OF AIR FLOWING BETWEEN PARALLEL PLATES

By

JOHN LOUIS GUILLORY

Bachelor of Science
University of Southwestern Louisiana
Lafayette, Louisiana
1962

Master of Science
Louisiana State University
Baton Rouge, Louisiana
1965

Submitted to the Faculty of the
Graduate College of the
Oklahoma State University
in partial fulfillment of
the requirements for
the Degree of
DOCTOR OF PHILOSOPHY
May, 1973

OKLAHOMA
STATE UNIVERSITY
LIBRARY

FEB 15 1974

DEHUMIDIFICATION OF AIR FLOWING BETWEEN PARALLEL PLATES

Thesis Approved:

Thesis Adviser

Dean of the Graduate College

873279

PREFACE

This study is concerned with the influence of moisture deposition on the heat and mass transfer characteristics of a simple dehumidifying exchanger model. Analysis of the governing conservation equations (without the deposition effect) is made by integrating the equations in the "Lewis Number Unity" form but using actual numerical values of the Schmidt and Prandtl numbers. These analytical predictions are compared with experimental data obtained from condensing and noncondensing tests.

Probably few students have managed to complete their academic careers without at least once feeling that anything which they accomplished was in spite of rather than with the help of those around them. I am no exception. But, in the cold logic of reality, there is no doubt that without the unfailing encouragement of everyone with whom I have been associated in the past three years, this study could never have been completed.

I wish to express my appreciation to my major adviser, Dr. F. C. McQuiston, for his guidance and assistance, often above and beyond what was required of him, throughout this study. I also wish to express my gratitude to the other members of my committee, Dr. J. A. Wiebelt, Dr. J. D. Parker and Dr. K. J. Bell for their technical advice and

encouragement.

I also wish to take this means of thanking Mr. George Cooper of the Mechanical Engineering Laboratory for his advice and assistance during the construction of the test apparatus. The fact that it operated in a very satisfactory manner from the time it was first started (and the fact that I started and finished this study with the same number of fingers and toes!) may be credited in no small measure to Mr. Cooper.

Finally, I wish to note my special gratitude to my wife, Beverly, and my daughter, Lori, who sacrificed not only the material things I could have otherwise given them but also the personal time properly expected of a husband and father. I consider the extra encouragement and understanding during the past three years a loan which I plan to repay with interest.

TABLE OF CONTENTS

LIST OF TABLES

LIST OF FIGURES

NOMENCLATURE

English Letter Symbols

A	Area
b	One-half distance between plates
C_p	Specific heat at constant pressure
D	Hydraulic diameter, 4(flow area)/perimeter
f	Fanning friction factor
G	Mass velocity ($\dot{M}/A$)
g	Gravitational acceleration
h	Surface convective heat transfer coefficient
i	Enthalpy
j	Colburn j-factor
K	Convective mass transfer coefficient
k	Thermal conductivity
L	Length
Le	Lewis number (Pr/Sc)
$\dot{M}$	Mass flow rate
m	Concentration
Nu	Nusselt number (as used in this work, $h_i D/\Gamma$)
P	Pressure
Pr	Prandtl number ($C_p \mu/k$)
Q	Total heat transfer rate
Re	Reynolds number ($D\bar{U}\rho/\mu$)

Sc	Schmidt number (μ/γ)
t	Temperature
U	Overall heat transfer coefficient; Velocity at a particular location (e.g. U_c is centerline velocity)
$\bar{U}$	Average (bulk) velocity in flow direction
u	Local velocity component in flow direction
v	Local velocity component normal to flow direction; Specific volume

Greek Letter Symbols

α	Thermal diffusivity ($k/\rho C_p$)
Γ	Thermal diffusion coefficient (k/C_p)
γ	Mass diffusion coefficient (See Appendix A)
Δ	Thermal boundary layer thickness
δ	Momentum boundary layer thickness
η	Concentration boundary layer thickness
μ	Absolute viscosity
ν	Kinematic viscosity (μ/ρ)
ρ	Density
σ	Ratio of free area to total area (See Fanning friction factor calculation, Appendix D)
ω	Specific humidity

Subscripts

c	Centerline
db	Dry bulb
e	Entrance condition
eq	Equivalent

f	Property of saturated liquid
fg	Property associated with liquid-vapor phase change
g	Property of saturated vapor
h	Hydraulic
i	Interface; Total transfer (i.e. based on an enthalpy potential)
L	Liquid
m	Mean; Mass transfer (i.e. based on a concentration potential)
o	Exit condition
s	Surface of condensate
t	Sensible transfer (i.e. based on a temperature potential)
v	Vapor; Velocity
w	Wall
wb	Wet bulb

CHAPTER I

INTRODUCTION

The problem of predicting heat and mass transfer rates during removal of a condensable vapor from a non-condensable gas finds considerable application in the chemical process industry. However, in terms of the number of square feet of exchanger surface produced each year, one of the single largest applications of dehumidifying exchangers is in refrigeration and comfort air conditioning systems.

Man's earliest attempts to lower the temperature of some part of his environment did not require the use of heat exchangers in the modern sense. At least five centuries before Christ, the Egyptians made use of a combination of evaporative and interstellar radiational cooling to produce modest quantities of ice and cold water [1]* .[1] The first recorded use of natural ice for temperature control has been traced to

---

* Numbers in brackets refer to bibliography

---

[1] An unglazed earthenware vessel of water was placed on a rooftop after sundown. Slaves fanned the vessel through the night and skimmed the film of ice that formed. Reference [1] relates that Richard the Lionhearted received a frozen sherbet made by this process from Saladin, his adversary during the Crusades. Such a feat in the Asian desert must have been impressive but it is not recorded whether Richard was sufficiently Lionhearted to consume an aparatif presented by a man sworn to kill him!

Alexander the Great in Persia about 330 B.C. who made use of snow-packed trenches to cool wine for his legions [2].

Primitive refrigeration machinery was under development in the 18th century. Early designs used to refrigerate sea-going meat storage vessels were mostly open-cycle air machines using reversed steam engines for the compressors. A practical closed-cycle machine was patented in 1834 [1].[2]

Increasing interest in environmental applications of refrigeration equipment in the 1920's and 1930's led to the development of the finned evaporator still in wide use today [2]. Although this development made possible the compact evaporators needed to cool large quantities of air at low velocities and pressure drops, their design became almost exclusively a "cut and try" process due to the increased complexity of the convection and conduction phenomena associated with these units.

The purpose of this work is to study one particular problem associated with finned evaporators, that of predicting the effect of moisture deposition on finned surfaces.[3]

---

[2]Jacob Perkins, an American engineer, developed this machine using ether as the working fluid. He was one of the earliest designers to use a two-phase refrigerant and introduced the terms "condenser" and "evaporator". The machine was patented in England but never achieved any great degree of commercial success.

[3]In the interest of clarity and brevity of the problem statement, references will be deleted. Chapter II contains a detailed literature survey.

It has been recognized for some time that, for a given temperature difference, a finned evaporator will operate more effectively (i.e. it will transfer more sensible heat) if dehumidification is occurring simultaneously. The obvious explanation is that deposition of moisture on the surface of the exchanger (as drops, a wavy film or some combination of the two) disturbs the boundary layer in the same fashion that wavy or louvered fins do. Although this is a generally accepted explanation, experimental work has been limited to either impractically simple configurations or ordinary evaporators with such "extra" factors as bypass air and refrigerant tube spacing which tend to cloud the significance of the findings. In addition, real evaporator configurations practically defy realistic mathematical comparisons. In view of the need for a better means of predicting the phenomena of heat and mass transfer enhancement due to moisture deposition, the following program was established:

1. Mathematically analyze simultaneous heat and mass transfer for humid air flowing betweem parallel flat plates. The solution must be sufficiently simple to make parametric studies possible yet be sensitive to the effect of mass transfer on sensible heat transfer.

2. Use predictions from step (1) to design a closed loop device capable of measuring actual

performance of an exchanger configuration similar to the mathematical model.

3. Obtain data relating to heat transfer, mass transfer and frictional characteristics. Present in terms of the total (enthalpy) Colburn j-factor, total Nusselt number, sensible j-factor, mass transfer j-factor and Fanning friction factor. Compare to dry (non-condensing) tests and to analytical predictions of the performance of the same exchanger.

CHAPTER II

LITERATURE SURVEY

Although this paper is primarily concerned with the influence of moisture deposition on condensation, literature on this specific subject depends heavily on the body of literature in the general area of condensation heat and mass transfer. Therefore, this chapter is subdivided into the areas of pure component condensation, mixture condensation, exchanger design and moisture effects.

Pure Component Condensation

Even though exchangers designed specifically for condensation service have been built for well over a century, the first analytical investigation of this phenomenon is usually credited to Nusselt in 1916 [3]. His model was a vertical flat plate held at a constant temperature below the saturation temperature of the surrounding vapor (Figure 1). By assuming that the weight of the condensed fluid is balanced only by shear stresses at the wall, he derived an expression for the velocity profile in the condensate layer of the type

$$u = \frac{\rho}{2\mu}\delta^2\left[2\frac{y}{\delta} - \frac{y^2}{\delta^2}\right]$$

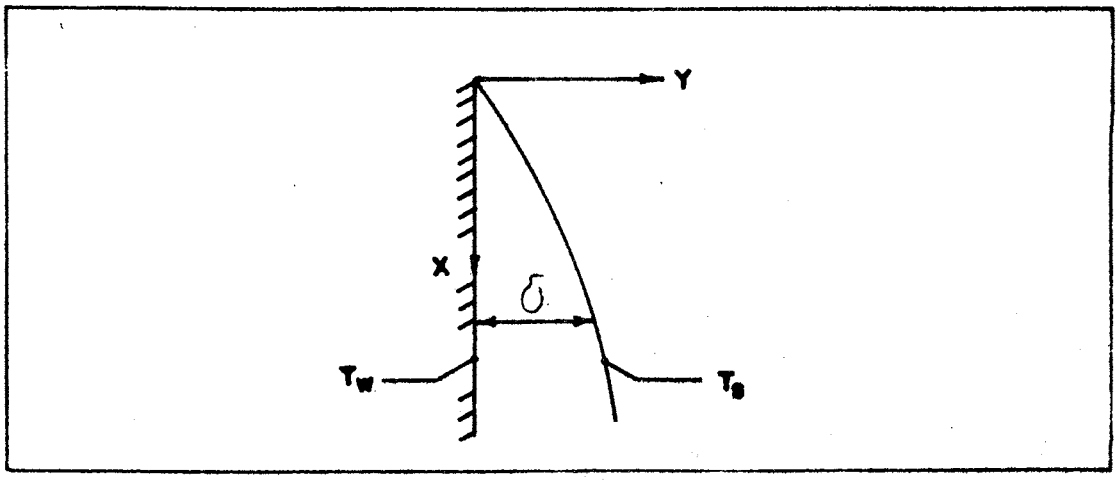

Figure 1. Nusselt Pure Component Condensation Model

This made possible relationships for the mass flow of condensate in terms of both mean velocity and thermal parameters. These expressions resulted in a differential equation for δ which has the solution

$$\delta = \sqrt[4]{\frac{4\nu k\,(t_s - t_w)\,x}{\rho\, i_{fg}}}$$

Heat transfer resistance was postulated to result only from the liquid film. Thus

$$h(x) = \frac{k}{\delta} = \sqrt[4]{\frac{k^3 \rho\, i_{fg}\, x^3}{4\nu (t_s - t_w)}}$$

Eckert and Drake [4] show the experimental validity of Nusselts result (reproduced in Figure 2) by plotting the actual Reynolds number

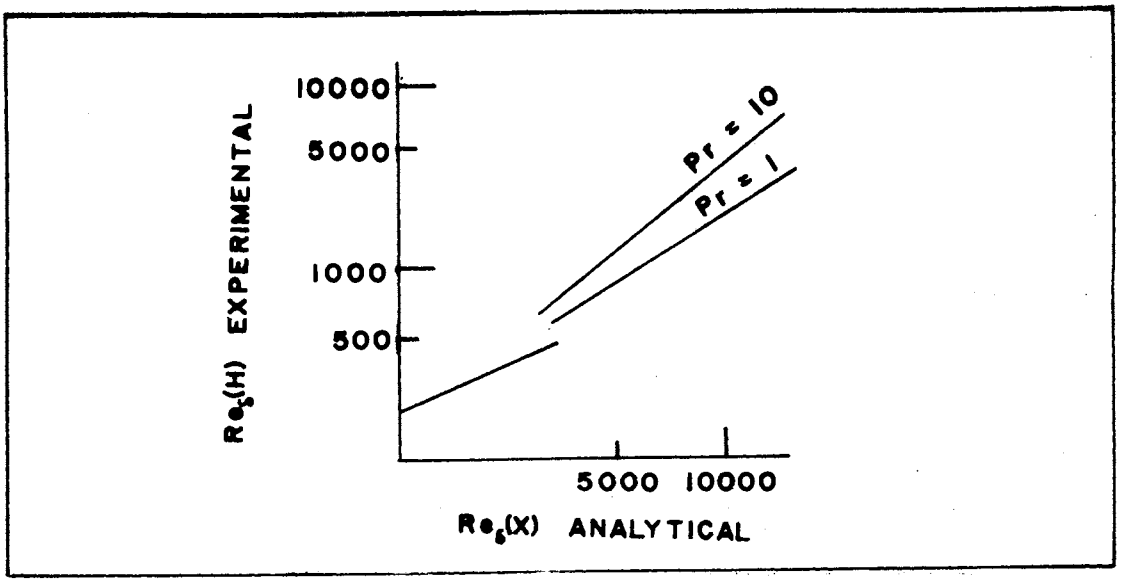

Figure 2. Experimental Comparison with Nusselt Analysis

$$Re_\delta(\text{experimental}) = \frac{\bar{h}\, x\, (t_s - t_w)}{\mu i_{fg}}$$

versus the result of Nusselt's analysis

$$Re_\delta(\text{analytical}) = \left[\frac{k\rho^{2/3} x\, (t_s - t_w)}{1.082\, i_{fg}\, \mu^{5/3}}\right]^{3/4}$$

Figure 2 illustrates that higher Reynolds numbers result in an increase in heat transfer not predicted by the Nusselt analysis. This is due to instability in the film at larger film thicknesses resulting in turbulent motion.

Sparrow and Gregg [5] developed a more precise analysis of the Nusselt problem by using boundary layer analysis (i.e. the differential forms of the mass, momentum and energy conservation equations) to account for the acceleration term deleted from the force balance in the original solution.

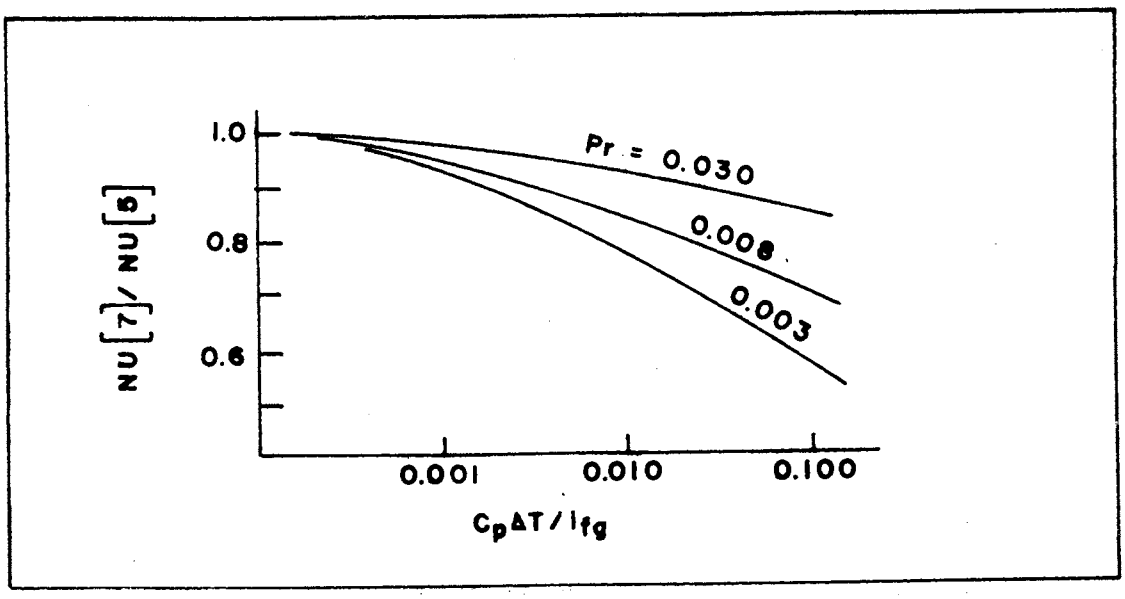

Figure 3. Sparrow and Gregg Analysis of Pure Vapor Condensation

This correction produces a Prandtl number dependence but is only significant at high heat rates and low Prandtl numbers as indicated in Figure 3. This correction also includes a buoyancy term neglected in the earlier analysis. The most important result of this analysis is that Nusselt's work is shown to be applicable over a wide range of fluids. This, when considered with the fact that the work of Sparrow and Gregg requires extensive numerical analysis of the boundary layer equations, makes Nusselt's solution quite attractive.

Several variations of Nusselt's original work appear in the literature. Koh solved the Nusselt-Sparrow-Gregg configuration by integral analysis but added no information to that already available [6]. Similar analyses of the horizontal plate problem (more generally, a plate normal to a

body force) have been made by Koh [7] and Leppert and Nimmo [8]. However, these studies do not have direct application to the present problem and are included merely to indicate the range of literature available in the general area.

There is an extensive body of literature available on experimental work in the field of pure vapor condensation which is especially important in those configurations that do not readily yield to analytical investigation. For instance, Beatty and Katz [9] correlated some 342 tests of pure component condensation on the outside of spiral-wound low-fin tubing and obtained the modified Nusselt equation

$$\bar{h} = 0.689\left[\frac{k_f^3 \rho_f^2 g\, i_{fg}}{\mu_f}\right]^{1/4}\left[\frac{1}{\Delta t_{vf}}\right]^{1/4}\left[\frac{1}{D_{eq}}\right]^{1/4}$$

Katz, Young and Balekjian extended this work to corrections for tube bundles [10].

Mixture Condensation

Whether by accident or design, many condensers must operate in the presence of a mixture of noncondensable gases or a mixture of condensable vapors that condense at varying rates. Performance tests on such devices show that the application of information derived for pure component condensation leaves much to be desired as a criterion for design. Sparrow and Lin [11] analyzed much the same problem as described in reference [5] with the addition of noncondensables to the vapor. The total heat transfer was shown

to follow the relation

$$\frac{Q}{i_{fg}\mu_L} = \frac{4}{3}\left[\frac{C_{pL}\,(t_i - t_w)}{i_{fg}Pr_L}\right]^{3/4}\left[\frac{g\,H^3}{4\,\nu_L^2}\right]^{1/4}$$

where H represents the height of the plate and t_i is the interface temperature which must be calculated by a trial and error procedure outlined in the reference. The results of such calculations are shown in Figure 4. This analysis predicts reductions in heat transfer on the order of 50% compared with the pure vapor case, a condition caused by the diffusion process being controlled by the concentration of the noncondensable near the surface of the exchanger. The physical mechanism is as follows: The general flow of the bulk mixture made necessary by the need for continuity with the condensate run-off carries with it the fraction of noncondensable present very far away from the plate. Since none of the noncondensable is assumed to be dissolved in the liquid phase of the condensable component, a steady state is eventually reached which is characterized by a high concentration of the noncondensable at the interface. This results in a depression of the vapor pressure of the condensable fraction below that at "infinity" thereby resulting in a lowered saturation temperature at the interface. Therefore, the effective temperature difference is lowered resulting in a lowering of the heat transfer rate compared to the case of the pure vapor.

In a later paper, Minkowycz and Sparrow reviewed the

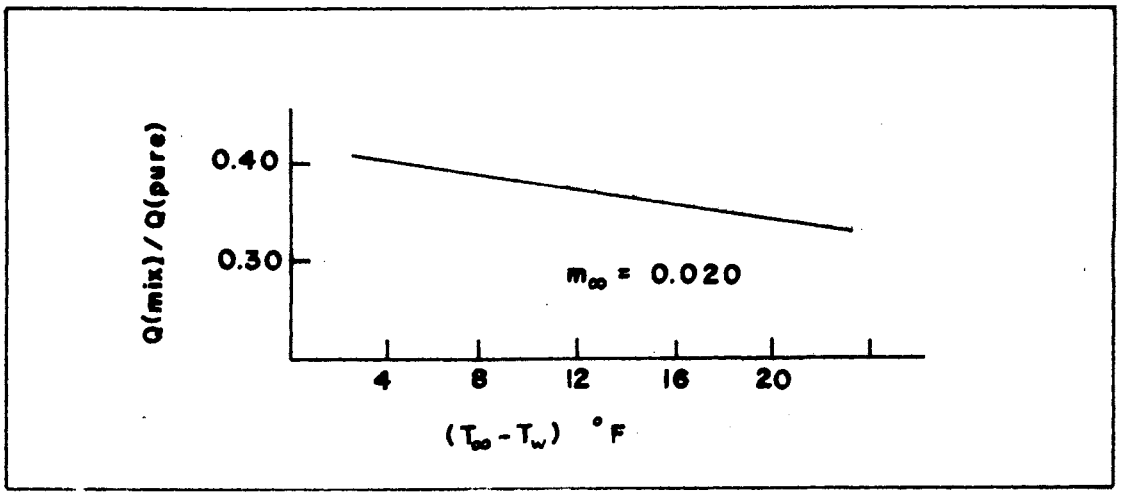

Figure 4. Sparrow and Lin Analysis of Condensation in the Presence of a Noncondensable

analytical state of the art concerning condensation on a flat plate [12]. Their analysis included, in addition to noncondensables, interfacial resistance and variable properties. This did not significantly change the results obtained in reference [11].

Although the studies cited up to this point provide valuable insight into the nature and mechanism of the condensation phenomenon, none attempt to model or predict the performance of actual condensers. For instance, the following items were not considered in any analysis referenced:

1. Bulk flow of the free stream

2. Possibility of forms of condensate run-off other than film type

3. Turbulent motion in condensate and/or bulk

4. Wall temperature variation[1]

Recognizing these limitations, Colburn approached the problem by means of experimental data correlation [13]. Using his own data as well as isolated experiments by other investigators involving a wide range of fluids (air, water, various hydrocarbons) and configurations (flow inside tubes, flow over tube banks, etc.), he was able to show that convective heat transfer in sensible systems could be correlated with the Reynolds number by the parameter

$$j_t = \left[\frac{h_t}{C_p\, G}\right] Pr^{2/3}$$

Another significant result of this work was proof of Reynolds' contention that heat transfer and friction data could be simply correlated. Colburn showed that this relation, in terms of his previously-defined 'j-factor', is

$$\frac{1}{2} f = j$$

where f is the Fanning friction factor. It should be stressed that this relation applies only to turbulent flow. Figure 5 shows the results of Colburn's correlations of j and f. Note that separate lines for heat transfer data and friction data are required in the laminar regime.

---

[1] References [9] and [11] treat finned tubes experimentally. However, these fins were quite short compared to the tube diameter and were accounted for by an "equivalent diameter" rather than an adjustment for wall temperature variation.

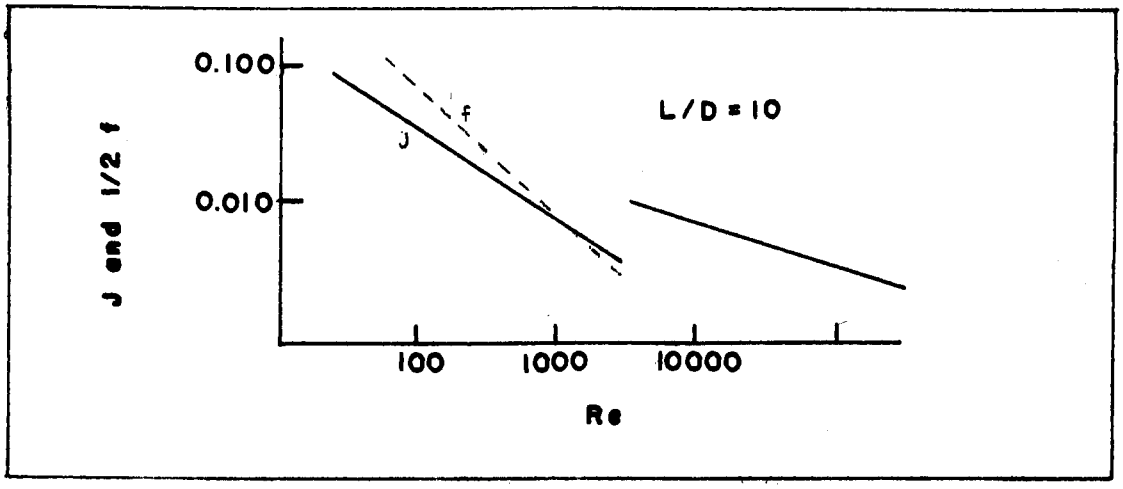

Figure 5. Colburn's Correlation of Heat Transfer and Friction Data for Flow Inside Tubes

The first extension of this work to condensation in mixtures was published by Colburn in 1934 [14]. Further details of this study were published the same year by Chilton and Colburn, the result being that a mass transfer j-factor could be defined in the same manner as the sensible j-factor and would correlate equally well with the Reynolds number [15].[2] This j-factor can be defined as

$$j_m = \left[\frac{K}{G}\right] Sc^{2/3}$$

---

[2]Chilton and Colburn's original formulation was

$$j_m = \left[\frac{K\ P_{fg}}{G}\right] Sc^{2/3}$$

based on a partial pressure potential. Concentration is now in more general use and will be used in this paper.

where K is a mass transfer coefficient based on some function of the concentration potential in the same manner that the heat transfer coefficient h describes heat transfer in conjunction with a temperature potential. Considerably less data were cited in the latter work than in Colburn's original paper on sensible correlations, especially in the laminar regime. No information was given to correlate j_t and j_m and theory only indicated that

$$j_t = C\ j_m$$

Since it was shown by experimental data that

$$C \approx 1$$

in the turbulent region, it was assumed that this was reasonably accurate in the viscous regime.

An extension of the condensation problem to the case of simultaneous condensation of mixed vapors was studied by Colburn and Drew [16]. Although primarily an analytical study, use of the j-factor for more than one condensing component is illustrated.

Various reviews are available outlining the state of the art in condensation heat and mass transfer which include extensive bibliographies. One such review by Berman is somewhat outdated but includes considerable emphasis on work in the Soviet Union, translations of which are difficult to find in other sources [17]. More recently, Chisholm and Leishman published a review including current work at the

National Engineering Laboratory in Great Britain and sixty references in the field [18].

Exchanger Design

The principal reason for basic studies in mixture condensation is the immediate problem of exchanger design. Therefore, design procedures were developed simultaneously with the theoretical investigations cited previously. For instance, Colburn and Hougen [19] published a method of surface area calculation for a condensing exchanger in the same issue that contained Chilton and Colburn's study of mass transfer j-factors. This method is a trial and error technique which requires that the feed stream be saturated and assumes that the sensible heat transfer j-factor and the mass transfer j-factor are identical. Examples are presented that indicate earlier methods (logarithmic mean temperature difference, for instance) result in as much as 100% oversizing.

Goodman published a series of articles in 1938 and 1939 devoted to the design of coils used specifically as refrigeration evaporators [20]. He suggested that an overall heat transfer coefficient for a wet surface U_w be calculated by the relation

$$\frac{1}{U_w} = \frac{K_1}{h_{air}} + \frac{K_2}{h_{ref}}$$

where h_{air} is the surface coefficient for the same exchanger

under dry (noncondensing) conditions, h_{ref} is the coefficient on the refrigerant side and K_1 and K_2 are constants related to the conditions of the air and exchanger configuration. In this respect, this assumption parallels Colburn's method. However, Goodman noted that the proper potential for energy transfer should be a logarithmic mean enthalpy difference so that in the relation

$$Q = A\, U_w\, \Delta\theta$$

$\Delta\theta$ should be defined as

$$\Delta\theta = \frac{\Delta i_{large} - \Delta i_{small}}{\ln\left[\frac{\Delta i_{large}}{\Delta i_{small}}\right]}$$

(The reasoning and limitations relating to the use of the enthalpy potential will be discussed at length in the next chapter. Goodman merely chose it as a convenient way of expressing the change in latent as well as sensible energy.) Goodman was among the first to attempt any adjustment for wet coil efficiency. By use of a nomograph which allowed the estimation of surface temperature throughout the exchanger (presented in the second article of his series), he showed that the psychrometric path of air being cooled sensibly and dehumidified simultaneously should appear as shown in Figure 6. Although Goodman's work is somewhat dated by modern standards of technology, it is still widely used.

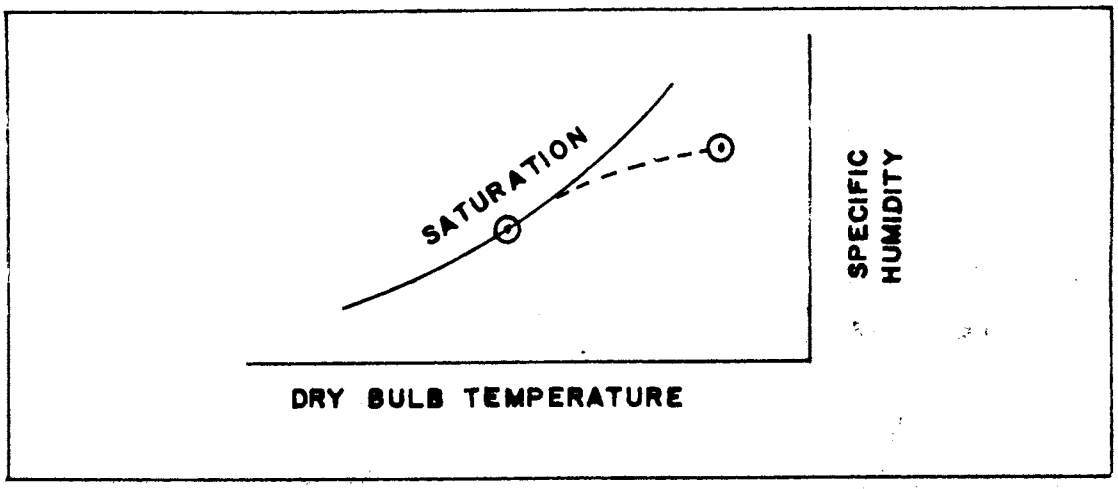

Figure 6. Psychrometric Path of Air in a Wet Coil (Goodman)

There are numerous modern refinements of the work initiated by Colburn and Goodman. Kusuda applied the effectiveness concept to wet coils [21]. McElgin and Wiley [22] and Wile [23] have updated the graphical approach. Bell has outlined a very detailed algorithm for sizing multi-component condensers [24]. ARI Standard 410 outlines accepted nomenclature, test procedures and data reduction for wet coils [25].

Influence of Moisture Deposition

The design procedures referenced in the preceding section are generally considered by the industry to be adequate. The nature of the design problem in the refrigeration coil industry is such that, while these procedures may not be perfect, further development is generally considered to be

of marginal value if that development results in increasing the complexity of the procedure. Therefore, the past few years have seen increasing interest in the refinement of input to these procedures. One such refinement that will be considered in detail here is the affect of moisture deposition on heat and mass transfer rates.

Trapanese, Bettanini and DiFilippo published findings in 1965 which indicated that a heat transfer coefficient calculated by means of an appropriate enthalpy potential is independent not only of the moisture content of the air but also of the ratio of sensible to total heat exchanged [26]. This conclusion, however, was based on relatively few tests of a commercial evaporator and should therefore be evaluated in qualitative rather than quantitative terms. In 1970, Bettanini published a study which allowed somewhat better interpretation of numerical results [27]. His experimental model consisted of a single vertical flat plate with a system for circulating (rather than forcing) flow near the plate. The purpose of the circulating system was to prevent buildup of dehumidified air near the surface and did not model most practical exchangers. However, his result confirmed a very interesting phenomenon which had been observed previously but never studied in such detail: When wet runs were made and a heat transfer coefficient based on total (sensible plus latent) heat transfer calculated, the result was 20% to 30% higher than when dry runs were made and the heat transfer coefficient calculated on a basis of sensible

heat transfer. Further, by spraying the wall with gypsum nodules in a configuration and size approximating condensate formation, he was able to reproduce the effect of wet runs in noncondensing tests. The results therefore indicated that the presence of condensate alone significantly increases the ability of a surface to transfer heat. This is especially interesting when it is recalled that Goodman suggested that the sensible heat transfer coefficient obtained from dry tests be used in calculations involving condensing systems. Yoshi, Yamamoto and Otaki have conducted similar tests of actual evaporator coils and report increases in the heat transfer coefficient on the order of 20% to 50% as well as pressure drop increases in the 50% range [28].

CHAPTER III

THEORETICAL ANALYSIS

The purpose of the analysis presented in this chapter is threefold:

1. To predict psychrometric conditions downstream from a given parallel plate condensing exchanger with sufficient accuracy to make possible a rational design of a test apparatus
2. To determine the parameters governing sensible heat transfer in a condensing system
3. To compute j-factors and Nusselt numbers obtained in this manner for subsequent comparison with empirical data

One of the most popular designs for refrigeration evaporator coils is the continuously finned type illustrated in Figure 7. For this type of exchanger, Kays and London show that the ratio of fin area to total (fin plus tube) area is on the order of 0.90 to 0.95 with air passage widths commonly less than one-eighth of an inch [29]. Jennings and Lewis state that bulk average air velocities are usually limited to about 1000 feet per minute due to power consumption and

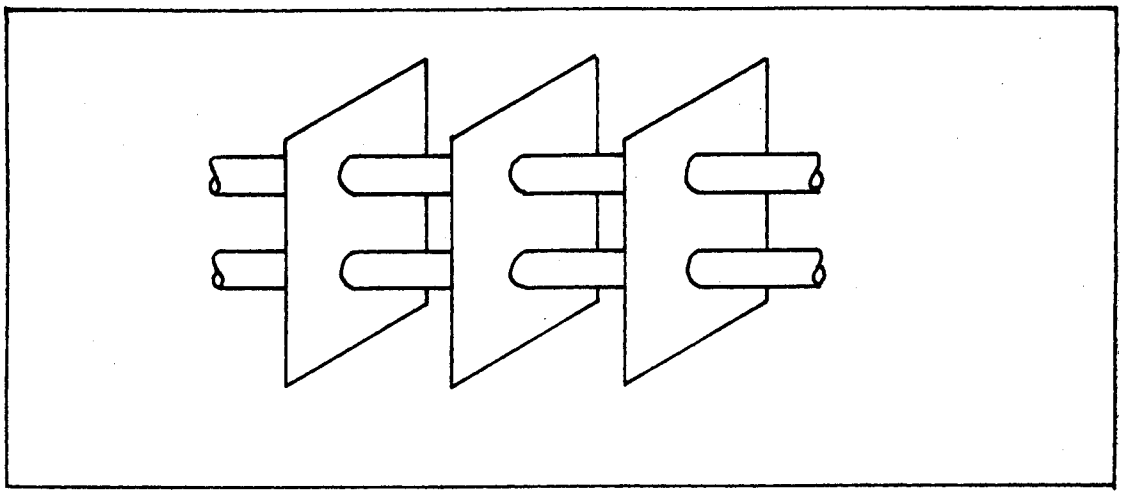

Figure 7. Continuously Finned Evaporator

noise considerations [30]. Assuming the physical properties of air to be those associated with common summer design conditions, a diameter Reynolds number of less than 1800 may be computed which indicates that the flow is in the laminar regime.

The length of flow passage required to obtain a fully-developed velocity profile is given by Kays [31] on page 63

$$L_v = D_h\left[\frac{Re}{20}\right] = 1.88 \text{ feet}$$

Likewise, the length of channel required to obtain a fully-developed dimensionless temperature profile is of the order

$$L_t = D_h\left[\frac{Re}{20}\right]Pr = 1.32 \text{ feet}$$

The dimensionless concentration profile becomes fully-developed at about

$$L_c = D_h\left[\frac{Re}{20}\right]Sc = 1.13 \text{ feet}$$

It would be unusual to find an evaporator of such depth in an ordinary system so this analysis must necessarily include entry-length effects.

The model to be analyzed is shown in Figure 8. No refrigeration tubes will be considered because of the hydrodynamic complexity that would be introduced as well as the difficulty of generalizing with two more parameters (tube diameter and spacing). The wall temperature will be considered to be constant at some value below the dew point of the mixture but above the frost point. Naturally, conduction in the fin will give rise to variations in the surface temperature of a real evaporator. Gardner [32] studied this problem extensively and ARI Standard 410 [25] describes the use of Gardner's work as applied to wet coils.

Air entering the passage ($x = 0$) will be assumed to be of uniform velocity with components only in the x-direction. Temperature and moisture concentration will also be considered uniform at the entrance. The temperature of the air will be limited to 125°F (thereby limiting the concentration of water vapor to 0.09 pounds of vapor per pound of mixture) in order to simplify the energy equation (this assumption, commonly known as the Lewis Number Unity assumption, will be

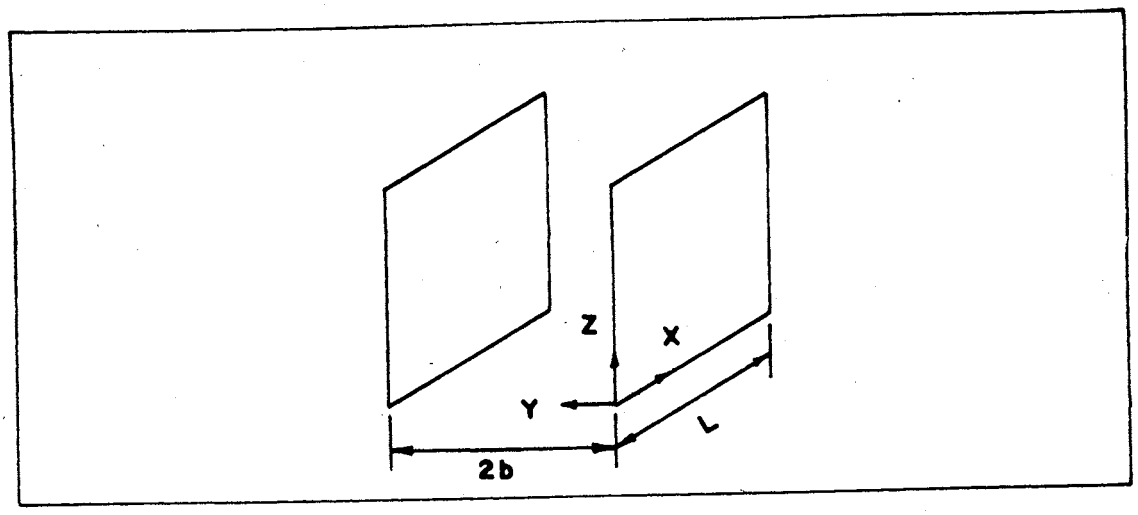

Figure 8. Analytical Model

discussed at length in Appendix A).

One of the most important limitations of this model is the lack of consideration of a condensate layer. As discussed in the preceeding chapter, this layer has significant effects on the heat transfer characteristics of a condensing system. This effect will be studied empirically later.

The momentum equation for this model is

$$u\frac{\partial u}{\partial x} + v\frac{\partial u}{\partial y} = -\frac{1}{\rho}\frac{\partial P}{\partial x} + \nu\frac{\partial^2 u}{\partial y^2} \quad \ldots\ldots\ldots\ldots \quad (1)$$

assuming constant properties and neglecting buoyancy effects. The continuity equation is

$$\frac{\partial u}{\partial x} + \frac{\partial v}{\partial y} = 0 \quad \ldots\ldots\ldots\ldots\ldots\ldots\ldots\ldots \quad (2)$$

under similar assumptions. Note that no extra equation is needed for moisture continuity since the boundary conditions

on this component are identical to that of the mixture.

The energy equation is

$$u\frac{\partial i}{\partial x} + v\frac{\partial i}{\partial y} - \frac{1}{\rho}\frac{\partial}{\partial y}\left[\sum_j \gamma_j \frac{\partial m_j}{\partial y} i_j\right] - \frac{k}{\rho}\frac{\partial^2 t}{\partial y^2} = 0 \quad \ldots\ldots\ldots\ldots \quad (3)$$

assuming constant properties and negligible heat and mass diffusion in the x-direction. Finally, the mass diffusion of water vapor through the mixture is given by

$$u\frac{\partial m}{\partial x} + v\frac{\partial m}{\partial y} - \frac{\gamma}{\rho}\frac{\partial^2 m}{\partial y^2} = 0 \quad \ldots\ldots\ldots\ldots\ldots\ldots \quad (4)$$

under conditions similar to those imposed on the energy equation.

Boundary conditions for this system of equations are

@ $x = 0$, $u = U$ (constant)

$v = 0$

$i = i_o$ (constant)

$m = m_o$ (constant)

@ $y = 0$, $u = v = 0$

$= 2b$ $i = i_w$ (a function of wall temperature)

$m = m_w$ (a function of wall temperature)

$t = t_w$ (constant)

@ $y = b$, $\partial / \partial y = 0$

In order to cast the energy equation in a more tractable form, a range of interest was previously defined limiting the

temperature of the air to 125°F. The reason for this limitation can be justified by Figure 9. This figure shows the dependence of the Prandtl number ($Pr = C_p \mu/k$) and the Schmidt number ($Sc = \mu/\gamma$) for air as a function of water vapor concentration. From this nomograph it can be seen that the Lewis number ($Le = Pr/Sc$) is less than 1.25 for temperatures below 125°F, an acceptable limit for most refrigeration applications. If, for mathematical simplicity, the ratio is taken to be exactly unity, it can be shown (see Appendix A) that the energy equation reduces to

$$u\frac{\partial i}{\partial x} + v\frac{\partial i}{\partial y} - \frac{\gamma}{\rho}\frac{\partial^2 i}{\partial y^2} = 0 \quad \ldots\ldots\ldots\ldots\ldots\ldots \quad (5)$$

for binary mixtures. This simplification not only eliminates the need for simultaneous solution of the energy and mass diffusion equations but indicates that both have the same solution mathematically. It can now be seen that Goodman's use of the enthalpy for the total energy transfer potential was an excellent choice since the simplified energy equation for a condensing system is identical to the equation governing sensible heat transfer in a noncondensing system with the enthalpy replacing the thermodynamic temperature.

The influence of mass transfer on sensible heat transfer becomes obvious upon inspection of equations (4) and (5). The enthalpy of an air-water vapor mixture can be given by an equation of the type

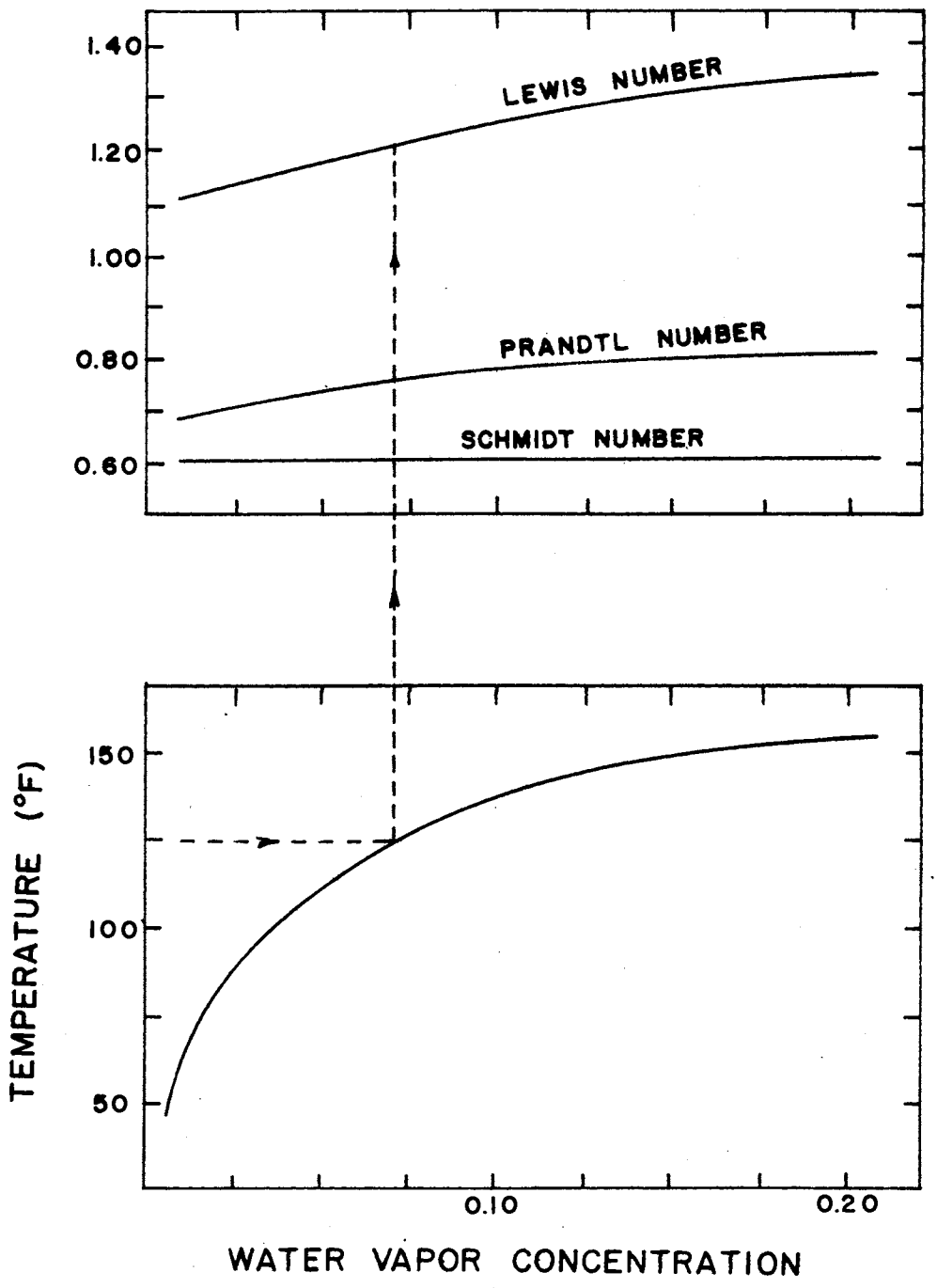

Figure 9. Selected Properties of Saturated Air-Water Vapor Mixture

$$i = C_{p_{air}} t + \frac{m}{1 - m}\left[i_g + C_{p_{H_2O}} t\right]$$

Therefore, the temperature profile t(y) is a function of both the enthalpy and concentration boundary conditions as is the sensible (Fourier) heat transfer.

It is now necessary to integrate equations (1), (2), (4) and (5) using boundary conditions given previously. Of the various methods that might be applied to these equations, the integral scheme was chosen for its simplicity and numerical flexibility.[1] The momentum equation may be rewritten (see, for instance, Goldstein [33]) as

$$\frac{d}{dx}\left[\int_0^{\delta} (U_c - u)u\,dy\right] + \frac{dU_c}{dx}\int_0^{\delta} (U_c - u)\,dy = \nu \frac{\partial u}{\partial y}\Big]_{y = 0} \qquad \ldots\ldots\ldots\ldots \quad (6)$$

where the pressure term is eliminated by the Bernoulli relation

$$U_c \frac{dU_c}{dx} = - \frac{1}{\rho} \frac{dP}{dx}$$

and all other pressure gradients neglected. The continuity

---

[1]This method as described in equations (14) through (37) has been applied with success to dry cases [34]. The details of this analysis are not included in other references and will therefore be presented here. Some modification to the earlier solution to the momentum equation is made. In order to study the dependence of sensible heat transfer on mass diffusion, the actual values of the Prandtl and Schmidt numbers will be used in the energy and mass diffusion equations even though the Lewis number is not precisely unity.

equation in integrated form is

$$\int_0^{\delta} (u - U_c)dy + b(U_c - \bar{U}) = 0 \quad \ldots\ldots\ldots\ldots\ldots \quad (7)$$

The energy and mass diffusion equations are both of the same form as the more commonly encountered energy equation in terms of the thermodynamic temperature

$$\frac{d}{dx}\left[\int_0^{\Delta} (t_e - t)udy\right] = \alpha \frac{\partial t}{\partial y}\Big]_{y=0} \quad \ldots\ldots\ldots\ldots \quad (8)$$

Therefore, by analogy,

$$\frac{d}{dx}\left[\int_0^{\eta} (m_e - m)udy\right] = \frac{\gamma}{\rho} \frac{\partial m}{\partial y}\Big]_{y=0} \quad \ldots\ldots\ldots\ldots \quad (9)$$

and

$$\frac{d}{dx}\left[\int_0^{\Delta} (i_e - i)udy\right] = \frac{k/C}{\rho} \frac{\partial i}{\partial y}\Big]_{y=0} \quad \ldots\ldots\ldots\ldots \quad (10)$$

The usual means of solving such a problem is to select a polynomial that will, as nearly as possible, satisfy the boundary conditions specified for the velocity profile and for each property profile. One such profile for use in the momentum equation is

$$u = U_c\left[2\left[\frac{y}{\delta}\right] - \left[\frac{y}{\delta}\right]^2\right] \quad 0 \leq y \leq \delta \quad \ldots\ldots\ldots \quad (11)$$

which was first suggested by Schiller (as reported in reference [34]).[2] Sparrow, among others, uses

$$\frac{i - i_w}{i_e - i_w} = \frac{3}{2}\left[\frac{y}{\Delta}\right] - \frac{1}{2}\left[\frac{y}{\Delta}\right]^3 \quad 0 \le y \le \Delta \quad \ldots\ldots \quad (12)$$

for the energy equation [34]. A similar expression will be used for the mass diffusion equation

$$\frac{m - m_w}{m_e - m_w} = \frac{3}{2}\left[\frac{y}{\eta}\right] - \frac{1}{2}\left[\frac{y}{\eta}\right]^3 \quad 0 \le y \le \eta \quad \ldots\ldots \quad (13)$$

By substituting the velocity profile from equation (11) into equation (7) and performing the indicated integration,

$$\delta/b = 3(1 - \bar{U}/U_c) \quad \ldots\ldots\ldots\ldots\ldots\ldots \quad (14)$$

Following a similar procedure with equation (6) and using equation (14) for δ,

$$dx = \frac{3}{10}\frac{b^2}{\nu}\frac{(U_c - \bar{U})(9U_c - 7\bar{U})}{U_c^2}\,dU_c \quad \ldots\ldots\ldots \quad (15)$$

Defining

$$x^* = \frac{x\nu}{b^2\bar{U}} = \frac{16(x/Dh)}{Re} \quad \ldots\ldots\ldots\ldots\ldots\ldots \quad (16)$$

$$U^* = U_c/\bar{U} \quad \ldots\ldots\ldots\ldots\ldots\ldots\ldots\ldots \quad (17)$$

---

[2] This relation does not satisfy the condition

$$\partial P/\partial x = \mu(\partial^2 u/\partial y^2) \quad @\ y = 0$$

imposed by the momentum equation at the wall. However, it adequately describes the variation in the centerline velocity in the x-direction which is the most important function of the momentum equation in this application.

and

$$\delta^* = \delta/b \quad \ldots\ldots\ldots\ldots\ldots\ldots\ldots\ldots \quad (18)$$

equations (14) and (15) may be expressed as

$$\delta^* = 3(1 - 1/U^*) \quad \ldots\ldots\ldots\ldots\ldots\ldots \quad (19)$$

and

$$dx^* = \frac{3}{10} \frac{U^* - 1}{U^{*2}} (9U^* - 7)\, dU^* \quad \ldots\ldots\ldots\ldots \quad (20)$$

The physical significance of the fact that both the Prandtl and Schmidt numbers are less than unity is that a certain portion of the outer enthalpy and concentration boundary layer profiles will be exposed to a flat velocity profile. Therefore, equations (9) and (10) may be written as

$$\frac{d}{dx}\left[\int_0^{\delta} (m_e - m)u\,dy + U_c \int_{\delta}^{\eta} (m_e - m)\,dy \right] = \frac{\gamma}{\rho} \frac{\partial m}{\partial y}\Big]_{y=0}$$

$\ldots\ldots\ldots$ (21)

and

$$\frac{d}{dx}\left[\int_0^{\delta} (i_e - i)u\,dy + U_c \int_{\delta}^{\Delta} (i_e - i)\,dy \right] = \frac{k/C}{\rho} \frac{\partial m}{\partial y}\Big]_{y=0}$$

$\ldots\ldots\ldots$ (22)

These equations may be written as differential equations of

the form

$$d\left[U^*\left[\frac{3}{8}\eta^* - \frac{1}{3}\delta^* + \frac{1}{8}\frac{\delta^{*2}}{\eta^*} - \frac{1}{120}\frac{\delta^{*4}}{\eta^{*3}}\right]\right] = \frac{3\gamma}{2\nu\rho}\frac{dx^*}{\eta^*} \quad \ldots\ldots\ldots\ldots\ldots\ldots \quad (23)$$

and

$$d\left[U^*\left[\frac{3}{8}\Delta^* - \frac{1}{3}\delta^* + \frac{1}{8}\frac{\delta^{*2}}{\Delta^*} - \frac{1}{120}\frac{\delta^{*4}}{\Delta^{*3}}\right]\right] = \frac{3\ k/C_p dx^*}{2\nu\rho\ \Delta^*} \quad \ldots\ldots\ldots\ldots\ldots\ldots \quad (24)$$

where

$$\eta^* = \eta/b \quad \ldots\ldots\ldots\ldots\ldots\ldots \quad (25)$$

and

$$\Delta^* = \Delta/b \quad \ldots\ldots\ldots\ldots\ldots\ldots \quad (26)$$

Solution of the momentum equation (20) can be accomplished in closed form by rewriting it as

$$\int_0^{x^*} dx^* = \frac{3}{10}\int_1^{U^*}(9 - 16/U^* + 7/U^{*2})dU^* \quad \ldots\ldots\ldots \quad (27)$$

or

$$x^* = \frac{3}{10}(9U^* - 16\ \ln(U^*) - 7/U^* - 2) \quad \ldots\ldots\ldots \quad (28)$$

The mass diffusion and energy equations cannot be integrated quite so easily both because of their forms and

because U^* cannot be given explicitly as a function of x^*. However, they can be rewritten as relatively simple first order linear differential equations by use of the identity

$$dx^* = (dx^*/dU^*)dU^* = dU^*/(dU^*/dx^*)$$

where dU^*/dx^* is given by equation (27). If this substitution is made into equation (23) and the differentiation performed as indicated, the following equation may be obtained after some algebraic manipulation:

$$\frac{dU^*}{d\eta^*} = \left[U^*\left[\frac{3}{8} - \frac{1}{8}\frac{\delta^{*2}}{\eta^{*2}} + \frac{1}{40}\frac{\delta^{*4}}{\eta^{*3}}\right]\right] \Bigg/ \left[\frac{9}{20\eta^* Sc}\left[9 - 16/U^* + 7/U^{*2}\right] - \left[\frac{3}{8}\eta^* - \frac{1}{3}\delta^* + \frac{1}{8}\frac{\delta^{*2}}{\eta^*} - \frac{1}{120}\frac{\delta^{*4}}{\eta^{*3}} + \frac{3}{4}\frac{\delta^*}{U^*\eta^*} - \frac{1}{10}\frac{\delta^{*3}}{\eta^{*3}U^*}\right]\right] \quad \ldots\ldots\ldots \quad (29)$$

In an identical manner, equation (24) may be transformed to

$$\frac{dU^*}{d\Delta^*} = \left[U^*\left[\frac{3}{8} - \frac{1}{8}\frac{\delta^{*2}}{\Delta^{*2}} + \frac{1}{40}\frac{\delta^{*4}}{\Delta^{*3}}\right]\right] \Bigg/ \left[\frac{9}{20\Delta^* Pr}\left[9 - 16/U^* + 7/U^{*2}\right] - \left[\frac{3}{8}\Delta^* - \frac{1}{3}\delta^* + \frac{1}{8}\frac{\delta^{*2}}{\Delta^*} - \frac{1}{120}\frac{\delta^{*4}}{\Delta^{*3}} + \frac{3}{4}\frac{\delta^*}{U^*\Delta^*} - \frac{1}{10}\frac{\delta^{*3}}{\Delta^{*3}U^*}\right]\right] \quad \ldots\ldots\ldots \quad (30)$$

It is now obvious that the advantage of transformation to

these somewhat formidable equations is that x^* no longer appears explicitly in the integration but only parametrically through U^* and δ^*. The equations to be solved are now simple first order relations.

The complete solution to equations (29) and (30) is best obtained numerically by use of the Runge-Kutta technique. The details of this solution are given in Appendix B but, briefly, it proceeds as follows:

1. Select a value of x^* corresponding to a point of interest (e.g. the exit).
2. Calculate the dimensionless centerline velocity U^* from equation (28).
3. Calculate dimensionless boundary layer thicknesses η^* and Δ^* from equations (29) and (30) by use of the Runge-Kutta technique.
4. Obtain polynomial expressions (12) and (13) for the enthalpy and concentration profiles.

In order to solve equations (29) and (30), it is necessary to obtain starting (boundary) conditions for $dU^*/d\eta^*$ and $dU^*/d\Delta^*$. Since equations (29) and (30) are mathematically identical, the forms of the expressions for the starting values will be the same. Therefore, only the value of $dU^*/d\Delta^*$ will be obtained here.

The starting point for all calculations will be the entrance to the exchanger ($x = 0$) which is characterized by a perfectly flat velocity profile (i.e. $U^* = 1$). Near this

location, the energy equation (24) may be integrated for $U^* \approx 1$. Further noting that equation (14) indicates that δ^* approaches zero as x^* approaches zero, an approximation of the behavior of Δ^* can be obtained from the simplified energy equation

$$d\left[\frac{3}{8}\Delta^*\right] = \frac{3}{2}\frac{\alpha}{\nu}\frac{dx^*}{\Delta^*} \quad \ldots\ldots\ldots\ldots\ldots\ldots \quad (31)$$

the solution of which is

$$\Delta^* = \sqrt{\frac{8x^*}{Pr}} \quad \ldots\ldots\ldots\ldots\ldots\ldots\ldots\ldots \quad (32)$$

Substituting the value of x^* from equation (32) into equation (28), the following relation between Δ^* and U^* can be obtained:

$$\frac{Pr}{8}\Delta^{*2} = \frac{3}{10}\left[9U^* - 16\ln(U^*) - 7/U^* - 2\right] \quad \ldots \quad (33)$$

from which

$$\frac{dU^*}{d\Delta^*} = \Delta^*\left[\frac{Pr}{2}\right] \Big/ \frac{3}{5}\left[9 - 16/U^* + 7/U^{*2}\right] \quad \ldots\ldots \quad (34)$$

This relation cannot be used as shown at $x^* = 0$ since it is of the indeterminate form 0/0. Applying L'Hospital's rule

$$\frac{dU^*}{d\Delta^*} = \left[\frac{Pr}{2}\right] \Big/ \left[\frac{3}{5}\left[16/U^* - 14/U^{*3}\right] dU^*/d\Delta^*\right] \quad \ldots \quad (35)$$

which, evaluated at $x^* = 0$ ($U^* = 1$), gives the relation

$$\frac{dU^*}{d\Delta^*} = \sqrt{\frac{5}{12}\,Pr} \quad \ldots\ldots\ldots\ldots\ldots\ldots\ldots \quad (36)$$

which is the required starting value. Similarly,

$$\frac{dU^*}{d\eta^*} = \sqrt{\frac{5}{12}\,Sc} \quad \ldots\ldots\ldots\ldots\ldots\ldots\ldots \quad (37)$$

With the information presented up to this point, it is possible to evaluate the thickness of the momentum, enthalpy and concentration boundary layers and the corresponding profiles. This, however, does not solve the problem of heat exchanger performance. It is therefore now necessary to evaluate the bulk psychrometric properties at any cross-section of the channel. For instance, the bulk (or mixing cup) enthalpy is defined as

$$i_m = \frac{1}{b\overline{U}} \int_0^b iu\,dy \quad \ldots\ldots\ldots\ldots\ldots\ldots\ldots \quad (38)$$

It is most convenient to separate the integral portion of this expression into three parts since the enthalpy boundary layer grows faster than the momentum boundary layer (since $Pr < 1$) and the profiles are not fully developed. This expression is

$$i_m = \frac{1}{b\overline{U}} \left[\int_0^{\delta} iu\,dy + \int_{\delta}^{\Delta} iu\,dy + \int_{\Delta}^{b} iu\,dy \right] \quad \ldots\ldots\ldots \quad (39)$$

Further simplification results from noting that, in the range between δ and Δ, U is a constant (equal to U_c) and, in the range between Δ and b, i is a constant as well (equal to i_e). Therefore

$$i_m = \frac{1}{b\bar{U}}\left[\int_0^{\delta} iu\,dy + U_c\int_{\delta}^{\Delta} i\,dy + U_c i_e(b - \Delta)\right] \quad \ldots \quad (40)$$

Substituting equation (12) for the enthalpy into the first and second integrals in equation (40) and equation (11) for the velocity into the first integral, the following polynomial expression may be obtained:

$$i_m = \frac{1}{b\bar{U}}\left[U_c\int_0^{\delta}(i_w + \left[(i_e - i_w)(\frac{3}{2}\left[\frac{y}{\Delta}\right] - \frac{1}{2}\left[\frac{y}{\Delta}\right]^3)\right])\cdot (2\left[\frac{y}{\delta}\right] - \left[\frac{y}{\delta}\right]^2)dy + U_c\int_{\delta}^{\Delta}(i_w + \left[(i_e - i_w)\cdot (\frac{3}{2}\left[\frac{y}{\Delta}\right] - \frac{1}{2}\left[\frac{y}{\Delta}\right]^3)\right])dy + U_c i_e(b - \Delta)\right] \quad \ldots \quad (41)$$

This expression consists exclusively of polynomials and may be integrated quite easily. The details, however, are somewhat lengthy and therefore only the result of the integration will be given here. Making the proper substitution of dimensionless variables

$$i_m = U^*\left[-\frac{1}{3}i_w\delta^* + (i_e - i_w)\delta^*(\frac{1}{120}\left[\frac{\delta^*}{\Delta^*}\right]^3 - \frac{1}{8}\left[\frac{\delta^*}{\Delta^*}\right]) + i_e - \frac{3}{8}(i_e - i_w)\Delta^*\right] \quad \ldots\ldots \quad (42)$$

Since the Schmidt number is also less than unity, an identical scheme can be used to obtain the mean concentration at any cross-section

$$m_m = U^*\left[-\frac{1}{3}m_w\delta^* + (m_e - m_w)\delta^*\left(\frac{1}{120}\left[\frac{\delta^*}{\eta^*}\right]^3 - \frac{1}{8}\left[\frac{\delta^*}{\eta^*}\right]\right) + m_e - \frac{3}{8}(m_e - m_w)\eta^*\right] \quad \ldots\ldots \quad (43)$$

Note that both these equations are merely functions of boundary conditions and the solutions of equations (28), (29) and (30). Since the mean enthalpy and mean concentration are independent thermodynamic properties of the mixture, any other thermodynamic variable may now be calculated by use of the appropriate equation of state. The details of determining such variables as dry bulb temperature and specific humidity are outlined in Appendix B.

The heat and mass transfer correlation parameters (Colburn j-factors) can now be obtained from simple energy and mass continuity balances across the exchanger. The total (sensible plus latent) heat transfer j-factor j_i is defined as

$$j_i = \left[\frac{h_i}{G}\right]Pr^{2/3} \quad \ldots\ldots\ldots\ldots\ldots\ldots\ldots \quad (44)$$

where h_i is the convective heat transfer coefficient based on an enthalpy potential and can be obtained from the energy balance

$$h_i A\left[\frac{i_i - i_o}{\ln\left[\frac{i_i - i_w}{i_o - i_w}\right]}\right] = \dot{M}(i_i - i_o) \quad \ldots\ldots\ldots\ldots \quad (45)$$

All enthalpies in equation (45) are mean rather than local

values.

The sensible heat transfer j-factor is defined as

$$j_t = \left[\frac{h_t}{C_p G}\right] Pr^{2/3} \quad \ldots\ldots\ldots\ldots\ldots\ldots\ldots \quad (46)$$

where the sensible heat transfer coefficient h_t is based on a thermodynamic temperature potential according to the energy balance

$$h_t A \left[\frac{t_i - t_o}{\ln\left[\frac{t_i - t_w}{t_o - t_w}\right]}\right] = \dot{M} C_p (t_i - t_o) \quad \ldots\ldots\ldots \quad (47)$$

In an analogous manner, the mass transfer j-factor j_m may be defined as

$$j_m = \left[\frac{K}{G}\right] Sc^{2/3} \quad \ldots\ldots\ldots\ldots\ldots\ldots\ldots \quad (48)$$

where the mass transfer coefficient K is based on a concentration potential as defined by the relation

$$KA \left[\frac{m_i - m_o}{\ln\left[\frac{m_i - m_w}{m_o - m_w}\right]}\right] = \dot{M}(m_i - m_o) \quad \ldots\ldots\ldots\ldots \quad (49)$$

There are existing solutions to which this procedure may be compared to illustrate its accuracy. For instance, Kays and London plot the sensible heat transfer Nusselt number

$$Nu_t = h_t \left[\frac{D}{k}\right]$$

versus the factor

$$\frac{2\ (x/D)}{Re\ Pr}$$

for a circular tube and show that all data reduces to a single curve (i.e. the parametric influence of the L/D ratio is completely expressed in the abscissa) [29]. For the case presently under consideration, the sensible plus latent heat transfer Nusselt number may be defined as

$$Nu_i = h_i\left[\frac{D_h}{\Gamma}\right] \qquad (50)$$

and plotted against

$$x^* = \frac{16\ (x/D)}{Re}$$

since x^* is a naturally-occuring parameter of this analysis (the horizontal scale used by Kays and London and that used here obviously differ only by a constant for a given Prandtl number). This graph is shown in Figure 10 and, in addition to exhibiting the "single curve" characteristic predicted by the Kays and London analysis, agrees precisely with the circular tube analysis at low values of x^* where the boundary layer is quite small compared to the distance between plates. At larger values of x^*, the solution is asymptotic to a mean Nusselt number of 7.54, the value recommended by many references for fully-developed flow between parallel plates (see, for example, reference [31], page 117).

A second immediate result of this analysis is a rational approximation of the locus of exit psychrometric conditions which may be expected when humid air passes through a heat exchanger, the surface of which is maintained below the dew point of the air. Previous investigators assumed a linear variation defined by a line connecting the entrance condition and the wall condition was adequate [20]. However, this analysis predicts two inflection points. Figure 11 shows a psychrometric plot for a given geometric configuration (L/D = 12) with fixed entrance and exit conditions and variable Reynolds number. The result is that, for higher Reynolds numbers, the process falls on the straight line described above. A decrease in Reynolds number tends to turn the curve downward but a further decrease causes the curve to turn once more back toward the wall condition resulting in an "S" shape.

The results of this analysis will be further illustrated in Chapter V. The following list reiterates the important assumptions made in this analysis:

1. Constant fluid properties
2. Laminar flow
3. Constant wall temperature
4. No effects due to condensate deposition

The fourth assumption is considered the most serious limitation and will subsequently be studied in detail experimentally.

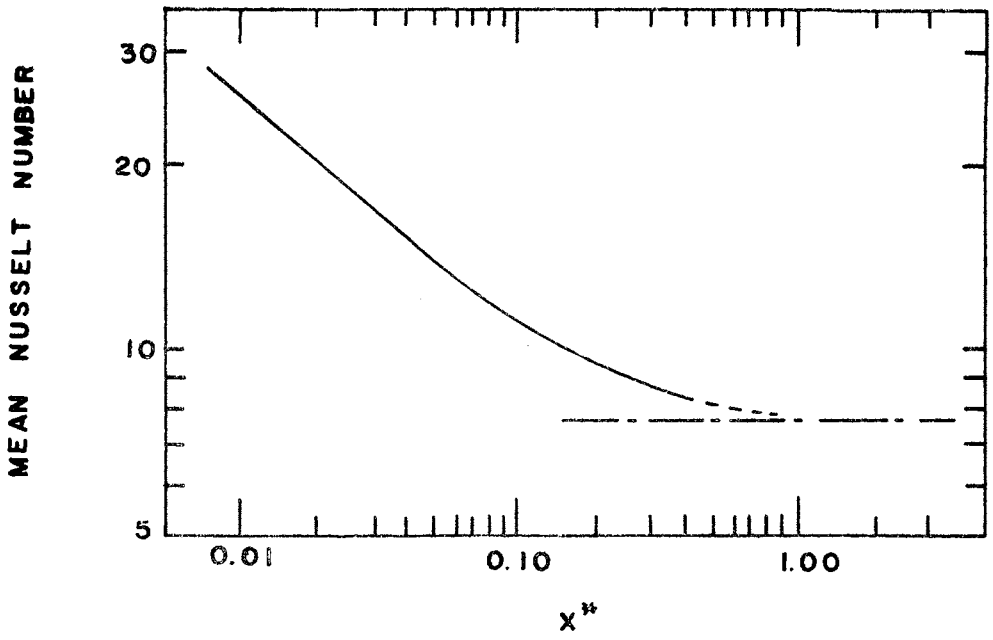

Figure 10. Mean Enthalpy Nusselt Number Obtained From Analysis

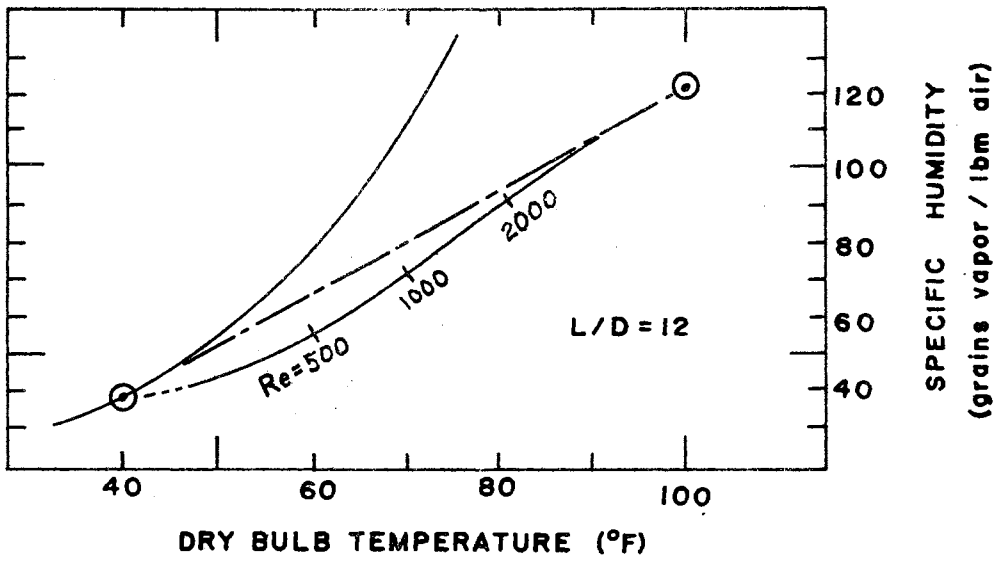

Figure 11. Psychrometric Path of Dehumidified Air Obtained From Analysis

CHAPTER IV

EXPERIMENTAL INVESTIGATION

Since several investigators [26, 27, 28] have indicated that moisture deposition alone significantly increases heat transfer coefficients, the analysis presented in Chapter III would be incomplete without some comparison with empirical data. The purpose of this chapter will be to outline briefly the means used to acquire this data. A detailed technical description of the apparatus is found in Appendix C.

When the need for data relating to wet exchanger surfaces became evident, contact was made with a large refrigeration equipment manufacturer, the result of which indicated that data were not available on any configuration approximating the analytical model; therefore, the device shown in Figure 12 was constructed to obtain data from a model similar to that used in the analytical study [35].

The apparatus operates as follows: A three-stage centrifugal blower provides air which passes through an electrical nichrome-ribbon heater (powered by a 220-volt auto-transformer). A vertical section in the duct provides a convenient means for removal of excess moisture added in the humidification section. After humidification, the flow is mixed and wet and dry bulb readings taken.

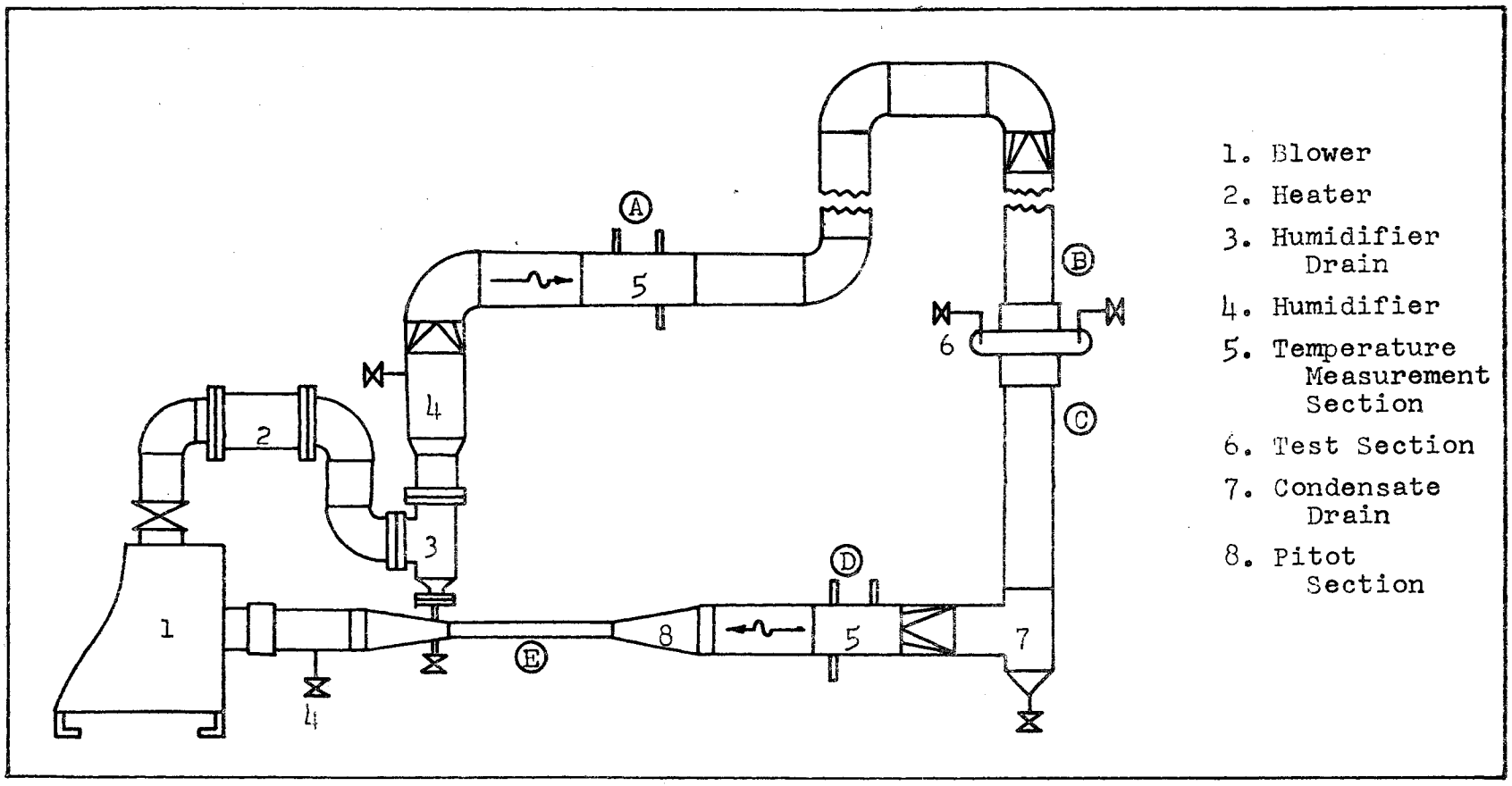

Figure 12. Schematic of Experimental Dehumidification Loop

Having thus obtained the desired psychrometric conditions, the flow is elevated as high as the ceiling of the room permits, turned vertically downward and passed through a series of aluminum honeycomb straighteners. Just prior to the test exchanger entrance, a final dry bulb reading is made to account for energy losses through the duct walls. The air then passes through a test exchanger composed of thirteen air passages of one-eighth inch width, six inch length and three inch height in the flow direction (note that the length-to-width ratio of 48 approximates the infinite flat plates studied analytically). The exchanger plates are cooled with refrigerated water of such a flow rate as to approximate the constant wall temperature condition. A second dry bulb temperature is measured downstream from the exchanger. The air then passes through a series of baffles which directs the air to a horizontal duct run and simultaneously removes moisture droplets formed on the exchanger walls. Psychrometric properties are measured again and a pitot-static tube is used to measure the flow rate. The air is then returned to the inlet of the blower.

The heat and mass transfer parameters described in Chapter III can now be calculated from the experimental data obtained as outlined above. Subscripts and functional dependence refer to the points shown on Figure 12. For example, the heat transfer coefficient based on an enthalpy potential as defined in equation (45) can be calculated thus:

$$h_i = \frac{\dot{M}(\Delta P_e,\ v_b)}{A} \ln\left[\frac{i(\omega_a,\ t_a) - i(t_w)}{i(\omega_d,\ t_c) - i(t_w)}\right]$$

All parameters given in equations (44) through (50) can be evaluated in a similar manner.

The pressure drop across the core can be easily measured and the Fanning friction factor calculated for comparison with the Reynolds analogy in this flow regime. Details of this calculation are presented in Appendix D.

CHAPTER V

COMPARISON OF ANALYTICAL AND EXPERIMENTAL RESULTS

This section is devoted to graphical presentations of the heat and mass transfer parameters obtained by analytical and experimental means. Subsections in this chapter deal with the behavior of the total (enthalpy) j-factor, the mass transfer j-factor, the sensible heat transfer j-factor, the Fanning friction factor and the Nusselt number. In appropriate cases, the relation between wet and dry operation is illustrated.

Total J-Factor

Figure 13 shows the relationship between the total heat transfer j-factor and the Reynolds number. The most striking observation concerning the relationship of the various curves on this plot is the reasonable agreement between dry tests and theoretical calculations (particularly as to the trend of the curves) contrasted to the relatively high values obtained in wet tests. Good agreement between analysis and dry tests was expected due to the relatively accurate modeling of the boundary layer (i.e. no roughening of the exchanger walls due to condensate deposition). The

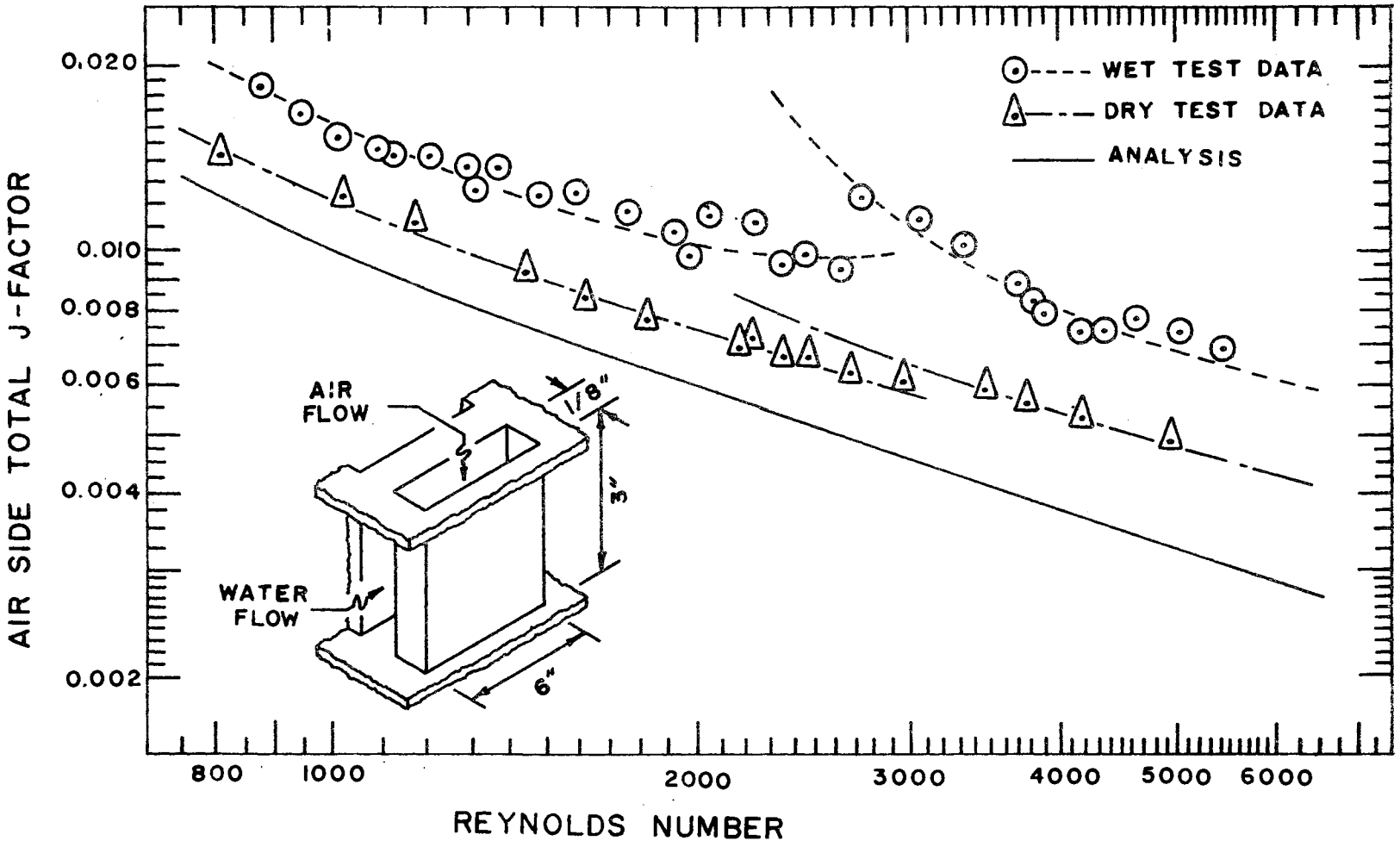

Figure 13. Total (Enthalpy Potential) J- Factors

differences that did occur are probably due to the thickness of the water passages causing unaccounted-for disturbances at the entrance to the air passages and to free-stream turbulence. It must therefore be concluded that moisture deposition is the major factor accounting for increases in the heat transfer coefficient. It can be shown that the only other factor differing in the wet and dry cases (mass diffusion) does not affect the value of j_i.[1]

Since the analysis considered laminar flow only, it should be expected that analytical and test results would show greater disagreement at higher Reynolds numbers. This is obviously the case in Figure 13.

These tests also showed that the rate of condensation has no influence on the value of the total j-factor. That is, for a given Reynolds number, the difference in the concentration of water vapor at the wall and in the free stream (which can be related to the rate of moisture deposition)

---

[1] In dry operation, the concentration of water vapor in the air is constant and the expression for the enthalpy of the air

$$i = C_{p_{air}} t + \omega i_{vapor}$$

reduces to

$$i = (C_{p_{air}} + \omega C_{p_{vapor}})t = \overline{C}_p t$$

Therefore, the solution for the enthalpy from equation (5), valid for the wet case, is identical to the solution for $(C_p t)$, valid for dry cases only. Substitution of this value into equation (45), however, does not affect the value of the enthalpy heat transfer coefficient and the resulting j_i is the same regardless of whether wet or dry operation is considered. This conclusion is, of course, subject to the Lewis Number Unity assumption.

does not affect the total heat transfer j-factor.[2] The explanation for this behavior lies in the fact that, at a given Reynolds number, a fixed quantity of condensate can be supported on the walls of the exchanger. Therefore, the rate at which it is deposited is merely reflected in the rate at which it runs off with the actual quantity of condensate on the walls at any given time (which represents the mechanism that enhances the j-factor) being relatively constant. The quantity and nature of the condensate on the surface will, of course, be strongly dependent upon the surface material, quantity and type of foreign materials on the surface, and many other factors. Such considerations therefore limit the general applicability of any one set of data.

A final comment on the comparison of wet and dry data concerns the transition region which, although difficult to study either analytically or with consistent empirical data, is commonly encountered in devices to which this work is applicable. It is apparent from Figure 13 that the onset of transition strongly affects data scatter in the wet tests while going practically unnoticed in the dry tests. Since the measurements made are relatively independent of flow

---

[2]The data scatter observed in the wet tests was considerably greater than in the dry tests. This scatter, however, proved to be random with respect to moisture content and is most likely a result of inaccuracies in measurement of temperatures in the wet runs. These measurements tended to be somewhat more difficult since the temperatures encountered were closer to the reference temperature and moisture was occasionally deposited on the thermocouples in certain locations.

regime, it can be concluded that moisture deposition significantly affects the flow regime in this region. In the dry case, movement away from the analytically predicted curve is relatively continuous in the Reynolds number range of 2000 to 3000, probably due to a continuous increase in the turbulent activity in the stream. In the wet case, however, droplet formation apparently tends to "trip" the stream into very turbulent motion much earlier than at the same Reynolds number in dry tests. This effect tends to produce a scatter of data rather than repeatable results in the transition region and should therefore not be considered a reliable phenomenon which can be depended upon for design purposes. It nevertheless represents one further example of the affect of condensate deposition upon flow characteristics.

Mass Transfer J-Factor

Figure 14 shows the result of theoretical and experimental calculations of the j-factor based on a concentration potential (j_m). The same general trends described in the discussion of the total heat transfer j-factor apply to this case. Data scatter is more pronounced in this portion of the test, probably a result of the particularly critical dependence upon the accuracy of the wet bulb readings. However, this scatter did not prove to be an important factor since it can be seen in Appendix E that "high" or "low" points do not share any particular characteristic (e.g. high or low condensation rate) consistently. This random

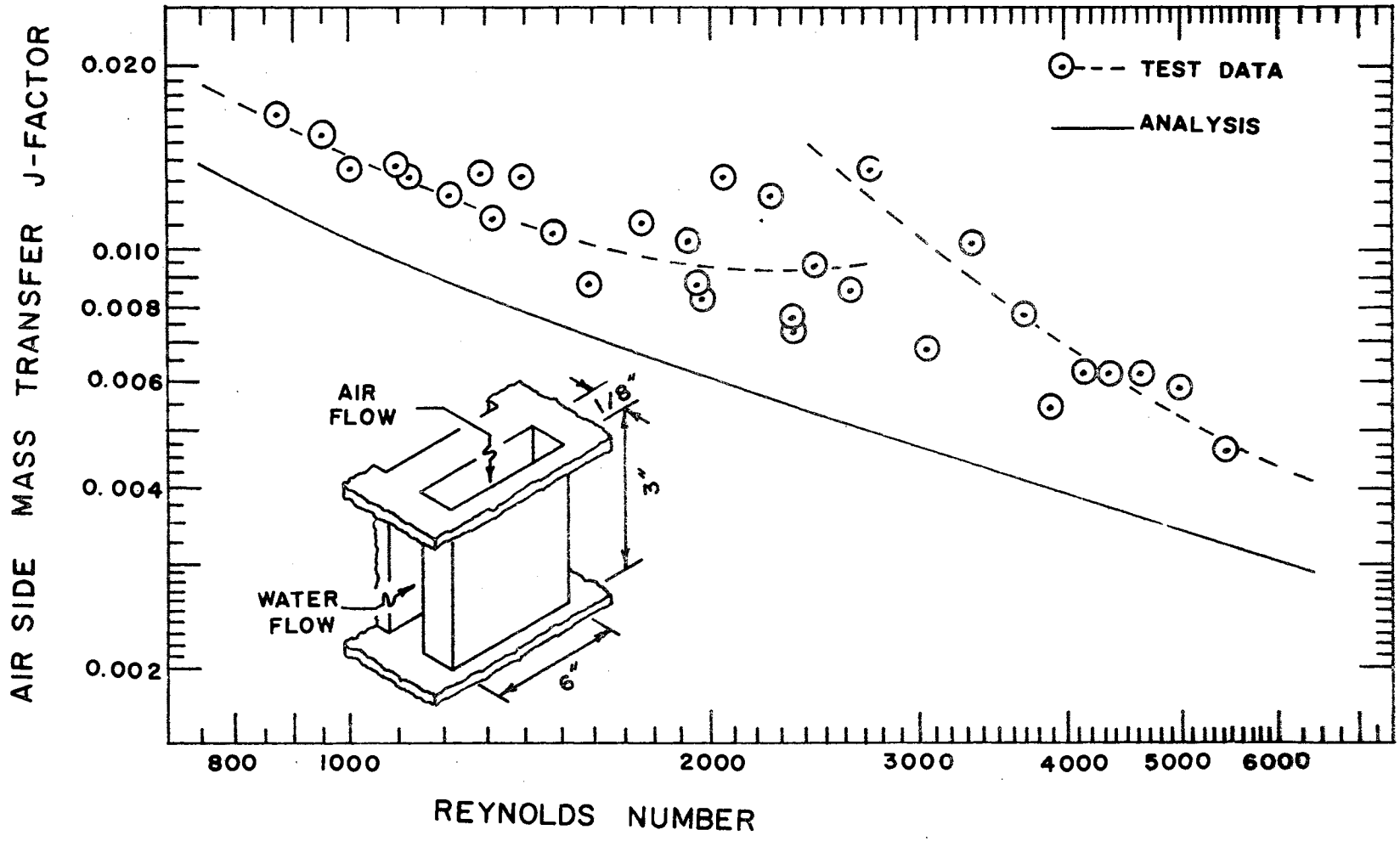

Figure 14. Mass Transfer (Concentration Potential) J-Factors

scatter did not cause any difficulty in fairing a single line through the data points. The transition effect is more pronounced than in the case of the total heat transfer j-factor but this could easily be a result of increased data scatter in the Reynolds number range of 2000 to 3000.

A particularly interesting result of comparisons between j_m and j_i is that the mass transfer j-factor is not increased by boundary layer disturbance in the same proportion as the enthalpy j-factor. Tests indicate that the increase in j_m above the analytically predicted value is more nearly comparable to the dry heat transfer j-factors than to the wet enthalpy j-factors. While this, in itself, indicates that flow disturbance is a factor in mass transfer rates, it also indicates that condensate deposition is not the major contributor to the increase. Therefore, although diffusion is ultimately the mechanism by which both energy and mass are transferred, condensate deposition tends to lower energy diffusion resistance to a greater degree than mass diffusion resistance.

Sensible J-Factor

Figure 15 shows the result of theoretical calculations of the sensible j-factor. Since a portion of the total heat transferred is a function of the moisture-dependent boundary conditions, the parameter

$$\phi = \frac{W_{in} - W_{out}}{2 W_w} \quad \ldots\ldots\ldots\ldots\ldots\ldots\ldots \quad (51)$$

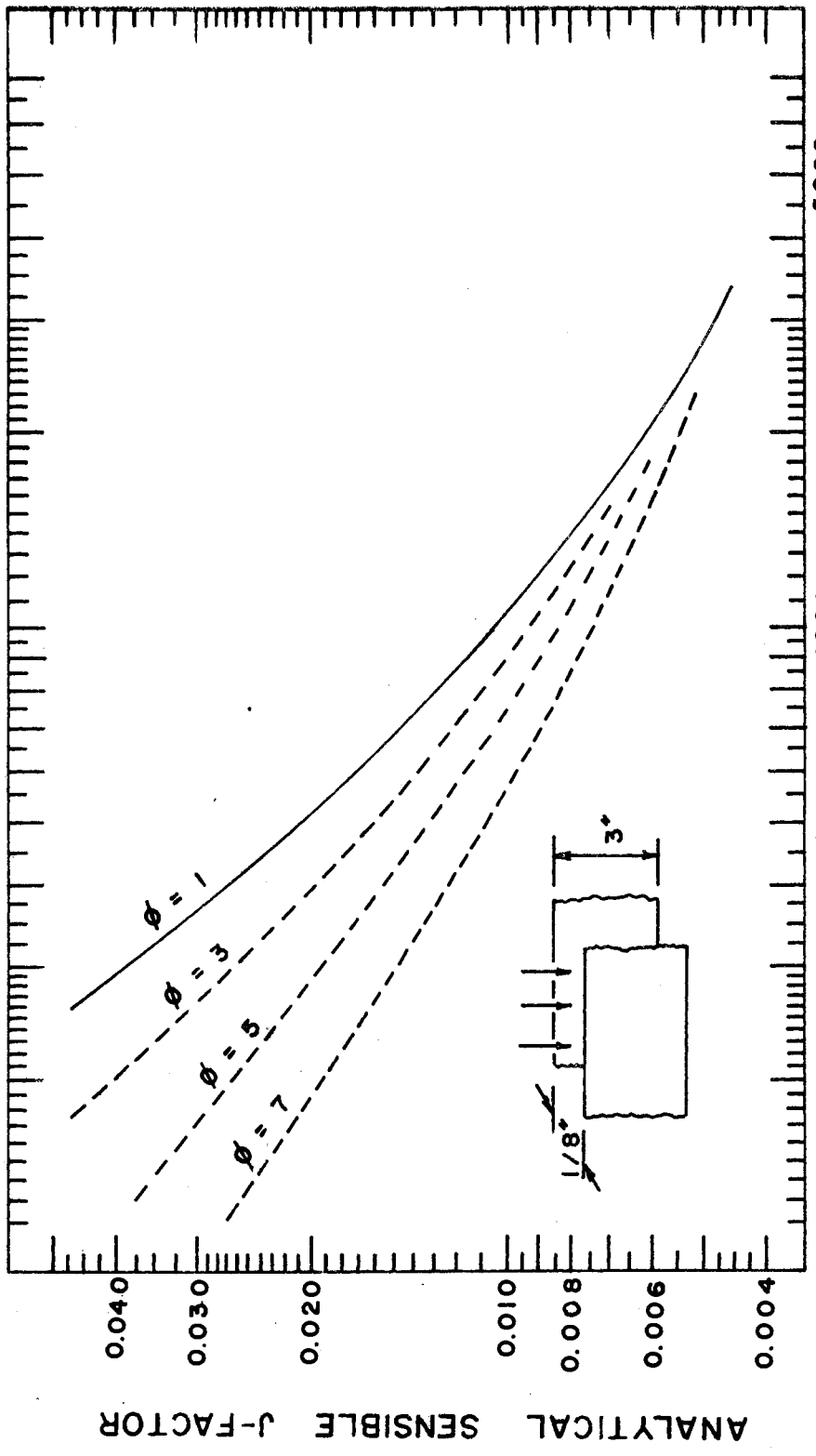

Figure 15. Sensible (Temperature Potential) J-Factors Obtained From Analysis

was selected for correlation purposes. This definition has the advantage of physical significance (the ratio of the arithmetic average of the bulk specific humidity to the specific humidity at the wall) and approaches unity for the case of wall temperatures above the dew point of the mixture (i.e. the dry case).

The values used to plot the curves in Figure 15 were obtained by parametric studies of the specific humidity boundary conditions. Since the Reynolds number can be considered an essentially independent variable, a plot of ϕ versus j_t for constant values of the Reynolds number was constructed from the parametric studies. A cross-plot of this graph was used to construct Figure 15.[3]

Figure 16 shows experimental sensible j-factors correlated with the same parameter ϕ discussed in the preceeding paragraph. Since ϕ varies with boundary conditions as well as the Reynolds number, each line of constant ϕ necessarily has relatively few points on it. Furthermore, since the value of ϕ for a given run cannot be controlled in the sense that the Reynolds number can, it was necessary to select a range of values of this parameter which, on the average,

---

[3]Forms of the correlation parameter ϕ other than the one used in Figure 15 were analyzed, e.g.

$$\phi' = \left[\omega_{in} - \omega_{out}\right] \Big/ \omega_w \ln \left[\frac{\omega_{in} - \omega_w}{\omega_{out} - \omega_w}\right]$$

but showed no particular advantage. The final decision was made based on the degree to which the correlation parameter separated data at a given Reynolds number.

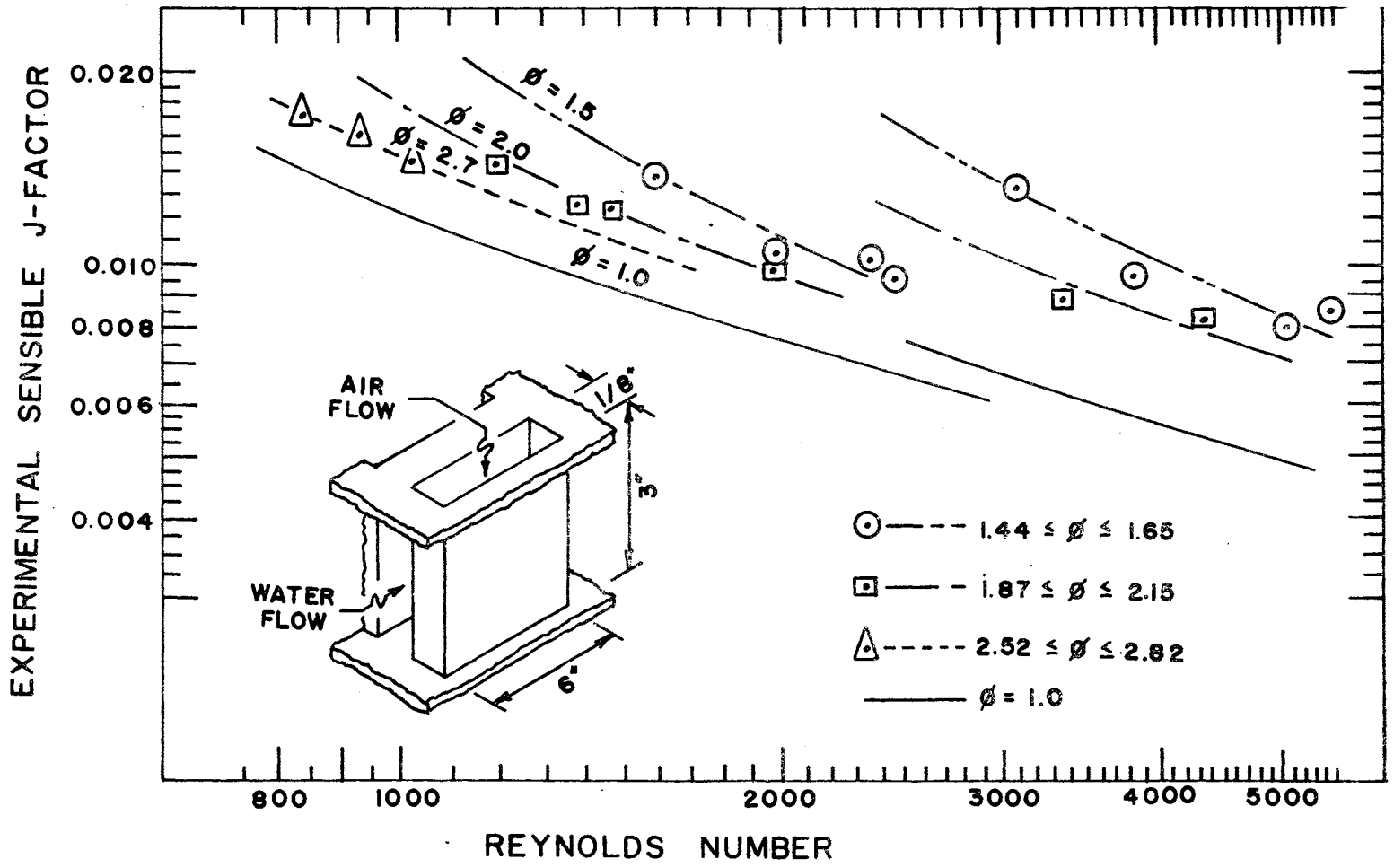

Figure 16. Sensible (Temperature Potential) J-Factors Obtained From Experiment

represented some desired value of ϕ. This, when combined with normal data scatter, tends to give a rather large data spread about the nominal curve. However, recognizing this and selecting nominal values of ϕ sufficiently separated, reasonably reliable curves may be faired through this data. The significance of these curves for design purposes will be discussed in Chapter VI.

Comparison of Figures 15 and 16 shows that the predicted relation between the curves of constant ϕ for $\phi > 1$ is the same in both cases, i.e., for a given Reynolds number, j_t is inversly proportional to ϕ. However, this relation is not continuous for the noncondensing case ($\phi = 1$) according to the test results but rather lies in the midst of the continuous family of curves $1 < \phi \leq \infty$.[4] The reason for this behavior must be the same as discussed previously in this chapter, i.e., disturbance of the boundary layer caused by moisture deposition. Obviously, this only influences cases where the deposition actually takes place ($1 < \phi \leq \infty$). Therefore, these curves are shifted upward while the curve representing $\phi = 1$ remains in the same location. It is interesting to note that this effect does not overshadow the

---

[4]This conclusion is substantiated by recognizing that larger values of ϕ represent cases where a larger portion of the total energy load on the exchanger is latent. Therefore, as ϕ approaches large values, the lines of constant ϕ approach the line $j_t = 0$. Since moisture deposition increases all heat transfer except in the dry case, it is logical to expect that some lines of constant ϕ will lie above the line $\phi = 1$ (as shown in this study) and some will lie below it.

trends predicted in Figure 15 but merely tends to shift the scale.[5]

Fanning Friction Factor

Although the particular analytical procedure used does not produce reliable pressure drop estimates (recall that arbitrary specification of a polynomial satisfying the velocity boundary conditions, while adequately describing the centerline velocity, does not meet the momentum equation requirements on the pressure gradient), the relation between heat transfer and friction data is of interest. Therefore, the pressure drop data taken in each run was used to calculate the Fanning friction factor. The relation between the friction factors obtained in wet and dry tests is shown in Figure 17. The increase in the friction factor due to condensate deposition in laminar flow is about 40% to 60% and in turbulent flow on the order of 30% to 50%. These results correspond closely to the findings of Yoshi et al [28].

Nusselt Number

The relation between the Nusselt number as defined in Chapter III for wet and dry tests of the exchanger described

---

[5] If noncondensing ($\phi = 1$) data were available for this exchanger with the surface artificially roughened (as in reference [27]), this data would lie above the line for $\phi = 1.5$ in Figure 16 and the curves would be continuous for $1 \leq \phi \leq \infty$ as predicted in Figure 15.

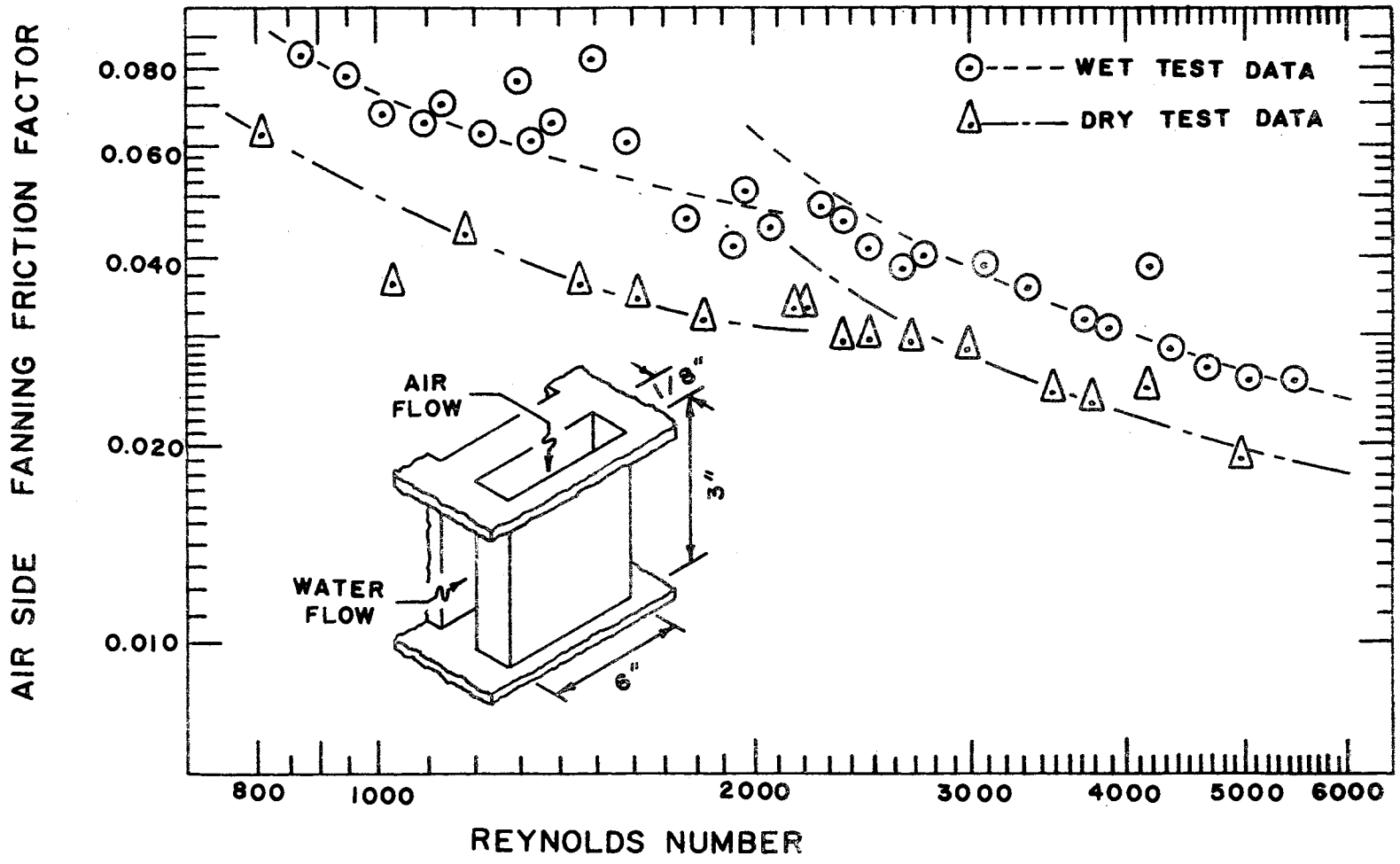

Figure 17. Fanning Friction Factors

in Chapter IV is shown in Figure 18. The conclusions concerning the Nusselt number are not significantly different fron those concerning the total j-factor. However, theory indicates that a single line should suffice regardless of geometry. Modifications to this theory are discussed in Chapter VI along with recommendations for the use of this data in the design of exchangers with L/D ratios other than the one tested in this study.

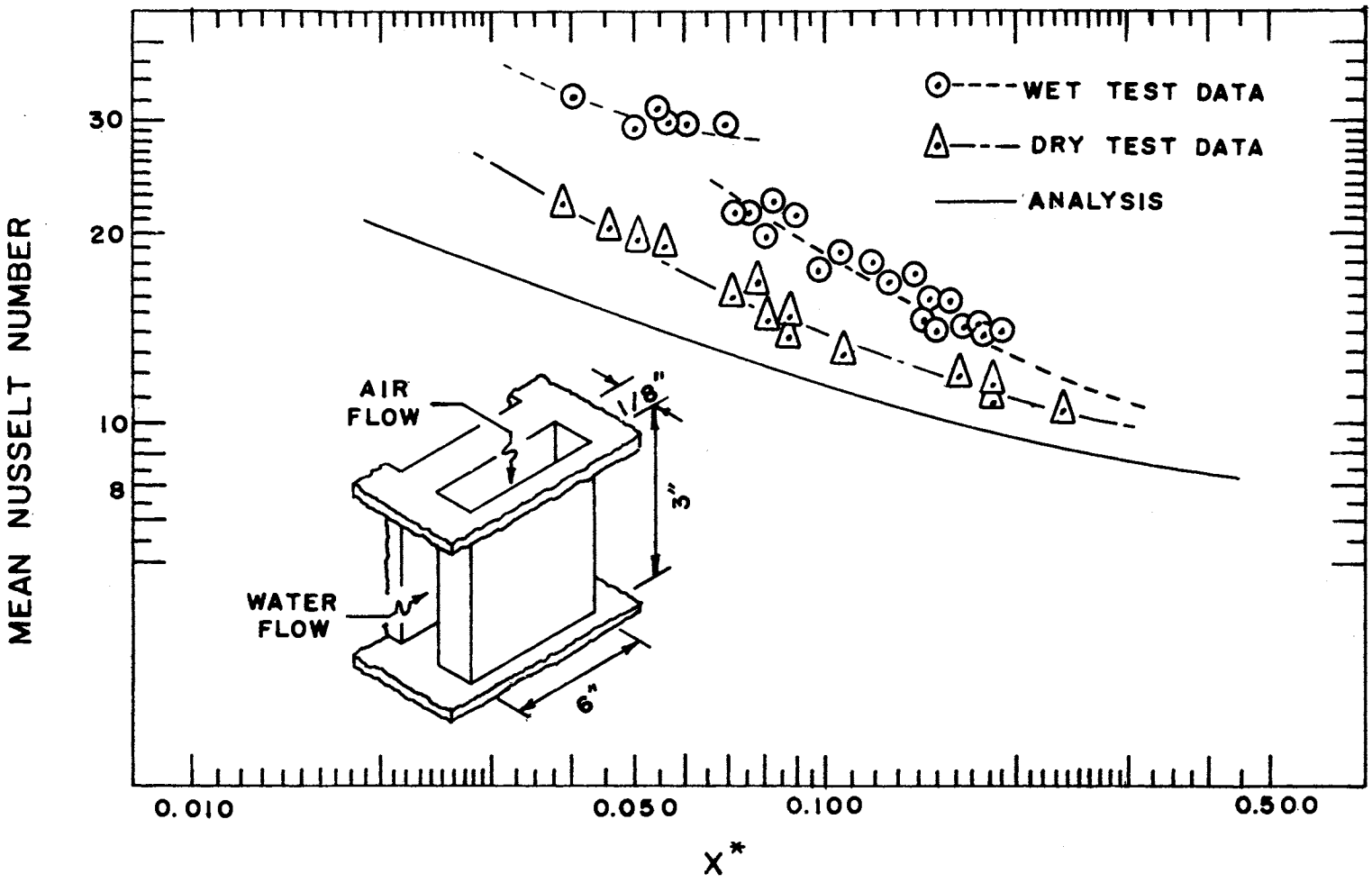

Figure 18. Mean Nusselt Numbers (Enthalpy Potential)

CHAPTER VI

CONCLUSIONS AND RECOMMENDATIONS

Many specific conclusions concerning both the analytical and experimental investigation have been discussed in previous chapters and will be briefly reviewed here. It should be emphasized that, although the results are presented in non-dimensional form, all empirical conclusions are based on a particular heat exchanger (L/D = 12) and should therefore not be freely applied to other geometries.

1. The analytical procedure developed in Chapter III adequately describes the j-factor trends in the Reynolds number range tested although actual numbers obtained by this method are unnecessarily conservative. The true total (enthalpy) j-factors are related to the theoretical values approximately as follows:

$$\frac{j_i(\text{actual})}{j_i(\text{theory})} = 1.59 + 2.91 \times 10^{-3}\left[\frac{Re}{1000}\right]^{5.23}$$

in the Reynolds number range between 800 and 2000 and by

$$\frac{j_i(\text{actual})}{j_i(\text{theory})} = 2.11 + 2.47 \times 10^{3}\left[\frac{Re}{1000}\right]^{-6.36}$$

in the Reynolds number range between 3000 and 6000. The corresponding equations for the mass transfer j-factors are

$$\frac{j_m(\text{actual})}{j_m(\text{theory})} = 1.32 + 1.94 \times 10^{-2}\left[\frac{Re}{1000}\right]^{3.47}$$

and

$$\frac{j_m(\text{actual})}{j_m(\text{theory})} = 1.27 + 8.05\left[\frac{Re}{1000}\right]^{-1.80}$$

for $800 \leq Re \leq 2000$ and $3000 \leq Re \leq 6000$, respectively.

2. The sensible j-factor in condensing operation varies with the parameter ϕ as indicated in Figure 16 and, like the enthalpy and concentration j-factors, is affected by condensate deposition. However, most practical refrigeration applications seldom encounter values of ϕ greater than two or three which makes correction for this factor often of little consequence in design calculations. By comparing Figures 13 and 16, it can be seen that a reasonable approximation for $1 \leq \phi \leq 3$ is

$$(j_t)_{wet} = (j_i)_{wet}$$

It is most important to recognize that, in wet operation, condensate deposition affects j_t in

a manner similar to j_i and that use of dry test data for j_t in designing equipment for wet operation can result in significant errors in performance prediction.

3. The influence of condensate deposition on the Fanning friction factor can be expressed by the relation

$$\frac{f(wet)}{f(dry)} = 1.23 + 0.246\left[\frac{Re}{1000}\right]^{0.25}$$

for $800 \leq Re < 2500$ and

$$\frac{f(wet)}{f(dry)} = 1.38 - 3.92 \times 10^{-4}\left[\frac{Re}{1000}\right]^{2.79}$$

for $2500 < Re \leq 6000$.

Further productive investigation could be conducted in several areas. Although considerable latitude is possible in psychrometric conditions, it has been shown that j_i and j_m are not affected by the rate of moisture deposition in the steady state. Therefore, efforts should be directed toward extending the range of Reynolds numbers, especially in the laminar regime. Data presented in this work can be reasonably extrapolated to cover most Reynolds numbers of practical interest.

Probably of more immediate importance is the testing of models with other L/D ratios. Figure 18 represents an

accepted means of expressing this effect since, in theory, one curve is sufficient. However, there is a possibility of an additional effect since the "average" thickness of the boundary layer relative to the disturbance size may be a factor.[1]

In order to study a model more nearly like those in common use, the effect of tubes may be simulated by pressing metal disks into the flow passages. This system would allow studies of the hydrodynamic effects on thermal performance caused by various tube sizes and configurations without the complications induced by non-uniform surface temperatures encountered in real evaporators.

Further studies should, of course, include actual

---

[1] In the absence of specific empirical data, some use may be made of the data in Figure 18 for the design of finned exchangers. For example, the presence of tubes or louvers may be considered to mix the flow periodically so that the actual exchanger may be approximated by a series of the simpler passages studied here. The L/D ratio (where L now represents the distance between disturbances in the flow direction) is commonly about five or six. Therefore, the boundary layer remains quite thin throughout the exchanger and the heat transfer characteristics of the exchanger tested in this work may therefore be considered to be a conservative approximation of many common evaporators.

Figure 18 indicates that the experimental Nusselt number tends to a constant value at large values of x^* as does the analytical curve, an important result since exchangers of this type often operate at quite low Reynolds numbers. Within the range of x^* tested, the ratio of the actual Nusselt number to the analytically obtained value decreases with increasing x^* and appears to approach unity at lower Reynolds numbers. In the absence of further empirical data, such exchangers should be designed on the basis of the more conservative analytical Nusselt number.

finned exchanger cores which would provide the effect of non-uniform surface temperature. Use of the work described in the preceeding paragraph would provide a means of studying the influence of the surface temperature distribution on exchanger performance.

It was shown in Chapters II and III that some disagreement exists concerning the psychrometric path of air undergoing dehumidification. A series of tests specifically designed to study this problem would be of value for comparison with the theory presented in this work. Data points presented herein reveal that actual conditions lie "below" curves such as shown in Figure 11. However, actual construction of curves for comparison purposes requires precise control of entrance and wall conditions as opposed to the wide range of conditions required for this study. Such curves would make polynomial or exponential fits of data possible which might prove simpler to use for purposes of predicting exchanger performance than the method presented in this work.

SELECTED BIBLIOGRAPHY

(1) Woolrich, W. R. The Men Who Created Cold New York: Exposition Press, 1967.

(2) Seventy-Five Years of Progress - The Frick Company Waynesboro, Pa., 1939.

(3) Nusselt, W. "Die Obertachen Kondensation des Wasserdampfes." Z. Ver. Dtsch. Ing., Vol. 60 (1916), 541-569.

(4) Eckert, E. R. G. and R. M. Drake, Jr. Heat and Mass Transfer New York: McGraw-Hill, 1959.

(5) Sparrow, E. M. and J. L. Gregg "A Boundary Layer Treatment of Laminar Film Condensation." Trans. ASME (J. Heat Transfer), Vol. 81 (1959), 13-18.

(6) Koh, J. C. Y. "An Integral Treatment of Two-Phase Boundary Layer in Film Condensation." Trans. ASME (J. Heat Transfer), Vol.83 (1961), 359-362.

(7) Koh, J. C. Y. "Film Condensation in a Forced-Convection Boundary Layer Flow." Int. J. Heat Mass Transfer, Vol. 5 (1962), 941-954

(8) Leppert, G. and B. Nimmo "Laminar Film Condensation on Surfaces Normal To Body or Inertial Forces." Trans. ASME (J. Heat Transfer), Vol. 90 (1968), 178-179.

(9) Beatty, K. O. and D. L. Katz "Condensation of Vapors On Outside of Finned Tubes." Chem. Engr. Prog., Vol. 44 (1948), 55-70.

(10) Katz, D. L., E. H. Young and G. Balekjian "Condensing Vapors on Finned Tubes." Pet. Refr., Vol. 33 (1954), 175-178.

(11) Sparrow, E. M. and S. H. Lin "Condensation Heat Transfer in the Presence of a Noncondensable Gas." Trans. ASME (J. Heat Transfer), Vol. 86 (1964), 430-436.

(12) Minkowycz, W. J. and E. M. Sparrow "Condensation Heat Transfer in the Presence of Noncondensables, Interfacial Resistance, Superheating, Variable Properties and Diffusion." Int. J. Heat Mass Transfer, Vol. 9 (1966), 1125-1144.

(13) Colburn, A. P. "A Method of Correlating Forced Convection Heat Transfer Data and a Comparison with Fluid Friction Data." Trans. AIChE, Vol. 29 (1933), 174-210.

(14) Colburn, A. P. "Calculation of Condensation with a Portion of Condensate Layer in Turbulent Motion." Ind. and Engr. Chem., Vol. 26 (1934), 432-434.

(15) Chilton, T. H. and A. P. Colburn "Mass Transfer (Absorption) Coefficients." Ind. and Engr. Chem., Vol. 26 (1934), 1183-1187.

(16) Colburn, A. P. and T. B. Drew "The Condensation of Mixed Vapors." Trans. AIChE, Vol. 33 (1937), 197-215.

(17) Berman, C. D. "The Heat and Mass Transfer During Vapor Condensation in the Presence of Noncondensing Gases." All-Union Heat-Engineering Institute, Vol. 8 (1947), 11-18. (Translation by Clearinghouse for Scientific and Technical Information, Springfield, Va.)

(18) Chisholm, D. and J. M. Leishman "Condensation in Surface Heat Exchangers." Chem. and Proc. Engr., (August, 1967), 160-164.

(19) Colburn, A. P. and O. A. Hougen "Design of Cooler Condensers for Mixtures of Vapors with Noncondensing Gases." Ind. and Engr. Chem., Vol. 26 (1934), 1178-1182.

(20) Goodman, W. "Performance of Coils for Dehumidifying Air." Heat. Pipe. and Air Cond., Vol. 10 (1938-1939), 8 articles.

(21) Kusuda, T. "Coil Performance Solutions without Trial and Error." Air Cond. Heat. and Vent., Vol. 57 (1960), 73-80.

(22) McElgin, J. and D. C. Wiley "Calculation of Coil Surface Areas for Air Cooling and Dehumidifying." Heat. Pipe. and Air Cond., Vol. 12 (1940), 195-201.

(23) Wile, D. D. "Air Coolin Coil Performance." Ref. Engr., Vol. 61 (1953), 727-732.

(24) Bell, K. J. "Algorithm for Partial/Multicomponent Condenser Design with a Superheated Feed." (Unpublished) School of Chemical Engineering, Oklahoma State University, Stillwater, Oklahoma

(25) "Standard for Forced-Convection Air-Cooling and Air-Heating Coils." Air Cond. and Ref. Inst., (1964)

(26) Trapanese, G. , E. Bettanini and P. DiFilippo "Essais Experimentaux sur l'Influence du Rapport Chaleur Sensible - Chaleur Totale sur le Coefficient de Transmission de Chaleur dans les Batteries de Tubes a Ailettes." Int. Inst Ref. Bul., Vol. 45 (1965), 323-339.

(27) Bettanini, E. "Simultaneous Heat and Mass Transfer On a Vertical Surface." Int. Inst. Ref. Bul., Vol. 70-1 (1970), 309-317.

(28) Yoshii, T. , M. Yamamoto and T. Otaki "Effects of Dropwise Condensate on Wet Surface Heat Transfer of Air Cooling Coils." Int. Inst. Ref. Bul., Preprint, 1971 Conference.

(29) Kays, W. M. and A. L. London Compact Heat Exchangers New York: McGraw-Hill, 1964.

(30) Jennings, B. H. and S. R. Lewis Air Conditioning and Refrigeration Scranton, Pa.: International, 1968.

(31) Kays, W. M. Convective Heat and Mass Transfer New York: McGraw-Hill, 1966.

(32) Gardner, K. A. "Efficiency of Extended Surfaces." Trans. ASME, Vol. 67 (1945), 621-631.

(33) Goldstein, S. (Ed.) Modern Developments in Fluid Mechanics, Volume I Oxford: Clarendon, 1938.

(34) Sparrow, E. M. "Analysis of Laminar Forced-Convection in Entrance Region of Flat Rectangular Ducts." NACA TN 3331 (1955)

(35) Private communication, Air Systems Development Division, Carrier Air Conditioning Company, Syracuse, New York (November 24, 1970).

(36) Rosenhan, A. K. "Psychrometric Chart Computer Subroutine." Obtained from Prof. J. A. Wiebelt, School of Mechanical and Aerospace Engineering, Oklahoma State University, Stillwater, Oklahoma.

(37) Jennings, B. H. Heating and Air Conditioning Scranton, Pa.: International, 1956.

(38) Jones, J. B. and G. E. Hawkins Engineering Thermodynamics New York: John Wiley, 1960.

(39) McQuiston, F. C. "Optimization of Fin-tube and Plate-Fin Surfaces Operating Under Conditions of Forced Convection." (Ph. D. Dissertation, Purdue University, 1970)

(40) Bird, R. B., W. E. Stewart and E. N. Lightfoot Transport Phenomena New York: John Wiley, 1960.

(41) Denny, V. E., A. F. Mills and V. J. Jusionis "Laminar Film Condensation From a Steam-Air Mixture Undergoing Forced Flow Down a Vertical Surface." ASME Paper 71-HT-E (1971).

(42) Gilles, R. and M. Douchez "Mass and Heat Transfer in Cooling and Dehumidifying Coils." Int. Inst. Ref. Paper 71-0878 (1971).

(43) Haas, J. C. and G. S. Springer "Mass Transfer Through Binary Gas Mixtures." ASME Paper 71-WA/HT-2 (1971).

(44) Kline, S. J. and F. A. McClintock "Describing Uncertainties in Single-Sample Experiments." Mech. Engr., Vol. 75 (January, 1953), 3-8.

(45) Ware, C. D. and T. H. Hacha "Heat Transfer from Humid Air to Fin and Tube Extended Surface Cooling Coils." ASME Paper 60-HT-17 (1960).

APPENDIX A

LEWIS NUMBER UNITY SIMPLIFICATION OF THE ENERGY EQUATION[1]

The differential equation expressing conservation of energy in a steady flow system with mass diffusion in the transverse direction involving two or more species is

$$G_x \frac{\partial i}{\partial x} + G_y \frac{\partial i}{\partial y} - \frac{\partial}{\partial y}\left[\sum_j \gamma_j \frac{\partial m_j}{\partial y} i_j \right] -$$

$$\frac{\partial}{\partial y}\left[k \frac{\partial t}{\partial y}\right] = 0$$

where γ_j is related to the diffusion coefficient D_j by

$$\gamma_j = \rho D_j$$

The final term in the energy equation represents conduction heat transfer due to the temperature difference in the y-direction and can be rewritten in terms of the various species that make up the system:

$$\frac{\partial}{\partial y}\left[k \frac{\partial t}{\partial y}\right] = \frac{\partial}{\partial y}\left[\Gamma c_p \frac{\partial t}{\partial y}\right] = \frac{\partial}{\partial y}\left[\Gamma \sum_j m_j c_j \frac{\partial t}{\partial y}\right]$$

---

[1]This simplification procedure can be found in many standard references. The procedure given here comes primarily from reference [33], page 302.

where Γ is the thermal diffusion coefficient

$$\Gamma = k/C_p$$

If the ideal gas assumption

$$C_j dt = di_j$$

is made, then

$$\frac{\partial}{\partial y}\left[k\frac{\partial t}{\partial y}\right] = \frac{\partial}{\partial y}\left[\Gamma \sum_j m_j \frac{\partial i_j}{\partial y}\right]$$

The Lewis number

$$Le_j = Pr/Sc_j$$

can also be written as

$$Le_j = \gamma_j/\Gamma$$

It can now be seen that if, for certain mixtures, $Le_j = 1$ (i.e. $\gamma_j = \Gamma$), the last two terms in the energy equation are

$$\frac{\partial}{\partial y}\left[\Gamma\left(\sum_j i_j \frac{\partial m_j}{\partial y} + \sum_j m_j \frac{\partial i_j}{\partial y}\right)\right]$$

which can be combined in a derivative form

$$\frac{\partial}{\partial y}\left[\Gamma \sum_j \frac{\partial}{\partial y}\left(m_j i_j\right)\right] = \frac{\partial}{\partial y}\left[\Gamma \frac{\partial i}{\partial y}\right]$$

The energy equation therefore reduces to

$$G_x \frac{\partial i}{\partial x} + G_y \frac{\partial i}{\partial y} - \frac{\partial}{\partial y}\left[\Gamma \frac{\partial i}{\partial y}\right] = 0$$

which is mathematically identical to the energy equation with no mass diffusion.

Although the Lewis number unity assumption restricts the number of mixtures that can be analyzed by this method, it is fortunate that one of the more common mixtures encountered in engineering design, air and water vapor, can be represented quite adequately.

APPENDIX B

NUMERICAL SOLUTION TO ANALYTICAL DESIGN EQUATIONS

This appendix will be devoted to a detailed description of the various calculation procedures leading to the solution of equations presented in Chapter III. The chronology of this section will follow that of the computer program shown in Table I.

Input Data

In keeping with the usual design specifications in work of this type, input data for the air stream is given in terms of the wet and dry bulb temperatures. Property input data required includes the Prandtl and Schmidt numbers. Data relating to exchanger dimensions includes provisions for solution at more than one value of exchanger depth in the flow direction in order to facilitate sizing. Other data specifications include air flow rate and wall temperature.

Thermodynamic Properties

Saturation Pressure Corresponding to a Temperature t [36]

$$P_g = 14.696 \left[218.167 \right] \times 10^{-y}$$

where

$$y = X\left[3.244 + \left(5.868 \times 10^{-3} + 1.170 \times 10^{-8} X^2\right)X\right] \Big/ \left[\left(((t - 32)/1.8) + 273.16 \quad 1\right)\left(2.188 \times 10^{3} X\right)\right]$$

and

$$X = 647.27 - \left[((t - 32)/1.8) + 273.16\right]$$

Vapor Pressure [37] , page 65

$$P_v = P_g(wb) - \left[\left(P_{air} - P_g(wb)\right)\left(t(db) - t(wb)\right) \Big/ \left(2800 - 1.3t(wb)\right)\right]$$

Specific Humidity and Concentration [38] , page 414

$$\omega = 0.622\left[P_v/(P_{air} - P_v)\right]$$

$$m = 1/(1 + 1/\omega)$$

Density [39] , page 151

$$\rho = 0.09734(1 + \omega)13.55P_b/\left[(1 \quad 1.607\omega)(t(db) + 460)\right]$$

where P_b is the barometric pressure measured in inches of Mercury.

Viscosity [39] , page 154

$$\mu = 0.0393742 + 6.79474 \times 10^{-5}\, t(db)^{-2} - 2.65385 \times 10^{-8}\, t(db)^2 \quad (lbm/ft\text{-}hr)$$

Enthalpy [37] , page 67

For t(db) less than or equal to 70°F,

$$i = 0.24t(db) + \frac{\omega}{1+\omega}\left[1061.7 + 0.439t(db)\right]$$

For t(db) greater than 70°F,

$$i = 0.24t(db) + \frac{\omega}{1+\omega}\left[1060.5 + 0.45t(db)\right]$$

Units of the above equations are BTU/lbm dry air.

Exit Boundary Conditions

Specification of the flow rate and passage dimensions make it possible to calculate the bulk velocity of the flow through the passage

$$\bar{U} = (CFM)/2bW$$

and the dimensionless passage length

$$x^* = x\,\nu/b^2\,\bar{U}$$

Equation (28) is then used to calculate the dimensionless core velocity U^*. Since U^* is not an explicit function of x^*, Newton's method is used to approximate the root of equation to within 10^{-6} of the actual value. After this solution is complete, the dimensionless boundary layer thickness δ^* is calculated from equation (19).

Concentration and Thermal Boundary Layer Thicknesses

The dimensionless concentration and thermal boundary layer thicknesses are given in the form of first order differential equations (29) and (30) with U^* as the independent variable. Starting with initial values of $dU^*/d\eta^*$ and $dU^*/d\Delta^*$ given by equations (36) and (37), equations (29) and (30) are solved using a fourth-order Runge-Kutta technique. The boundary layer thicknesses are incremented until such time as the solution for the local value of the dimensionless core velocity matches the value calculated previously.

Output Data

The calculations described above produce dimensionless thicknesses of the concentration and thermal boundary layers at the specified exit of the passage which are used to calculate the mixed mean concentration and enthalpy by use of equations (42) and (43). However, in the interest of producing data more easily plotted on a psychrometric chart, the mixed mean concentration is converted to specific humidity by the relation

$$\omega = \frac{1}{\left[\frac{1}{m} - 1\right]}$$

and equations of the type

$$i = C_{p_{air}} t(db) + \frac{1}{1 + \omega}\left[i_g + C_{p_{H_2O}} t(db)\right]$$

shown previously are used to calculate a mixed mean dry bulb temperature.

Other output data include equation (44) (total j-factor), equation (46) (sensible j-factor), equation (48) (mass transfer j-factor), equation (50) (Nusselt number), equation (51) (concentration ratio) and Reynolds number.

TABLE 1

COMPUTER PROGRAM FOR ANALYTICAL CALCULATIONS

1/5

```
      IMPLICIT REAL*8 (A-H,O-Z)
      REAL*8 ME,MW,IE,IW,IX
      DIMENSION RK(4),E(4),U(4),VAR(2),D(4),DTA(2),X(14)
C
C
C     OPTIONAL PRINT ROUTINE.........
C     IF A MORE COMPLETE RECORD OF STEPS INVOLVED IN SOLUTION IS DESIRED
C     PLACE A "1." IN THE FIRST COLUMN OF THE CARD IMMEDIATELY
C     FOLLOWING "$ENTRY".  OTHERWISE, PLACE A "0." IN THIS COLUMN.
C
C
C     INSERT DATA IN FOLLOWING ORDER.........
C     CARD #1 (EXCHANGER DATA) - PASSAGE WIDTH(INCHES), PASSAGE HEIGHT
C     (INCHES)
C     CARD #2 (PHYSICAL DATA) - PRANDTL NUMBER, SCHMIDT NUMBER,
C     SPECIFIC HEAT(BTU/LBM-F), THERMAL CONDUCTIVITY (BTU/HR-FT-F)
C     CARD #3 - NUMBER OF STATIONS (MAXIMUM 14)
C     CARD #4 - STATION POSITIONS (INCHES FROM ENTRANCE)
C     CARD #5 (PSYCHROMETRIC DATA) - ENTRANCE WET BULB TEMPERATURE
C     (DEGREES F), ENTRANCE DRY BULB TEMPERATURE (DEGREES F),
C     WALL TEMPERATURE (DEGREES F), FLOW RATE PER PASSAGE (CFM)
C
C
      READ(5,501)CHK
501   FORMAT(F10.5)
      ICHK=CHK+.001
      READ(5,500)WIDE,HGT
      READ(5,500)DTA(1),DTA(2),CP,COND
      READ(5,900)EN
      N=EN
      READ(5,901)(X(L),L=1,N)
536   READ(5,100)TE,TEDB,TW,CFM
      IF(TE.EQ.0.0)GOTO535
900   FORMAT(F10.5)
901   FORMAT(14F5.3)
500   FORMAT(4F10.5)
100   FORMAT(4F10.5)
      HOLD=0.
      HOLDM=0.
      CTH=0.
      CTHM=0.
      WRITE(6,200)
      WRITE(6,201)WIDE
      WRITE(6,202)HGT
      WRITE(6,204)CFM
      WRITE(6,205)
      WRITE(6,206)DTA(1),DTA(2)
      WRITE(6,207)CP,COND
C
C     SATURATION PRESSURE CORRESPONDING TO ENTRANCE WET BULB
C
450   TK=((TE-32.)/1.8)+273.16
      XX=647.27-TK
      Y=XX*(3.244+(5.86E-03+1.70E-08*XX**2)*XX)/(TK*(1.+2.188E-03*XX))
      PSEWB=14.696*218.167/(10.**Y)
C
C     ENTRANCE VAPOR PRESSURE (CARRIER EQUATION)
C
```

2/5

```
      VP=PSEWB-((14.696-PSEWB)*(TEDB-TE)/(2800.-1.3*TE))
C
C     SATURATION PRESSURE AT WALL
C
      TK=((TW-32.)/1.8)+273.16
      XX=647.27-TK
      Y=XX*(3.244+(5.86E-03+1.70E-08*XX**2)*XX)/(TK*(1.+2.188E-03*XX))
      PSWL=14.696*218.167/(10.**Y)
C
C     SPECIFIC HUMIDITIES
C
      SHE=.622*(VP/(14.696-VP))
      SHW=.622*(PSWL/(14.696-PSWL))
      EMU=(0.039374+6.794E-5*TEDB-2.653E-8*TEDB**2)
      DEN=.09734*((1.+SHE)/(1.+1.607*SHE))*13.55*29.92/(TEDB+460.)
      VISK=EMU/DEN
      WRITE(6,208)VISK
      WRITE(6,209)
      WRITE(6,210)TE
      WRITE(6,211)TEDB
      WRITE(6,212)TW
      REND=CFM*1440./(HGT*VISK)
      WRITE(6,351)REND
351   FORMAT(' REYNOLDS NUMBER = ',F7.0)
      IF(ICHK.EQ.1)WRITE(6,219)
      IF(ICHK.EQ.1)GOTO491
      WRITE(6,214)
      WRITE(6,350)
350   FORMAT(          ' POSITION     X*     DRY BULB  SP HUMID    PHI
     1      J(I)       J(M)       J(T)       NU(I)  */)
491   CONTINUE
C
C     ENTHALPIES
C
      IF(TEDB-70.)60,60,61
60    IE=(.24*TEDB+SHE*(1061.7+.439*TEDB))/(1.+SHE)
      GOTO62
61    IE=(.24*TEDB+SHE*(1060.5+.45*TEDB))/(1.+SHE)
62    IF(TW-70.)90,90,91
90    IW=(.24*TW+SHW*(1061.7+.439*TW))/(1.+SHW)
      GOTO92
91    IW=(.24*TW+SHW*(1060.5+.45*TW))/(1.+SHW)
92    CONTINUE
C
C     PASSAGE DATA
C
      UBAR=CFM*144./(WIDE*HGT)
      A=WIDE/24.
      ME=1./(1.+(1./SHE))
      MW=1./(1.+(1./SHW))
      DO999L=1,N
      XSTR=X(L)*VISK/(UBAR*720.*A**2)
      NT1=1.
      IF(ICHK.EQ.0)GOTO14
      WRITE(6,400)X(L),XSTR
400   FORMAT(///' X = ',F10.5,' INCHES,  X* = ',F10.5)
C
C     SOLUTION FOR DIMENSIONLESS CORE VELOCITY AND VELOCITY
```

```
C       BOUNDARY LAYER THICKNESS AT THE SPECIFIED LENGTH.
C
14      UT1=UT1+.001
        Y=XSTR-.3*(9.*UT1-16.*DLOG(UT1)-(7./UT1)-2.)
        IF(Y)11,15,14
11      UT1=UT1-(Y/(.3*(9.-16./UT1+7./UT1**2)))
        IF(Y.LT.0.0)0001)GOTO15
        Y=XSTR-.3*(9.*UT1-16.*DLOG(UT1)-(7./UT1)-2.)
        GOTO11
15      USC=UT1
        DSTR=3.*(1.-(1./USC))
        IF(ICHK.EQ.0)GOTO401
        WRITE(6,402)USC
402     FORMAT(/,' DIMENSIONLESS CORE VELOCITY = ',F10.5,//////)
        WRITE(6,403)
403     FORMAT(' RUNGE-KUTTA SOLUTION'//)
        WRITE(6,404)
404     FORMAT(' POSITION (E(4))     CORE VELOCITY (URK)'//)
C
C       RUNGE-KUTTA SOLUTION FOR DIMENSIONLESS CONCENTRATION AND
C       THERMAL BOUNDARY LAYER THICKNESSES.
C
401     DO70J=1,2
        IF(J.EQ.1)URK=HOLD
        IF(J.EQ.1)E(4)=CTH
        IF(J.EQ.2)URK=HOLDM
        IF(J.EQ.2)E(4)=CTHM
        H=0.0005
        IF(I-1)301,301,41
301     RK(1)=DSQRT(5.*DTA(J)/12.)
        E(1)=0.
        U(1)=1.
        DO271=2,4
        GOTO(30,30,33,34),I
30      E(2)=H/2.
        U(2)=1.+H*RK(1)/2.
        GOTO21
33      E(3)=H/2.
        U(3)=1.+H*RK(2)/2.
        GOTO21
34      E(4)=H
        U(4)=1.+H*RK(3)
21      D(I)=3.*(1.-(1./U(I)))
        R=D(I)/E(I)
        SC=DTA(J)
        RK(I)=U(I)*(.375-.125*R**2+.025*R**4)/((9.*(9.-(16./U(I))+
       1(7./U(I)**2))/(20.*E(I)*SC))-(.375*E(I)-(1./3.)*D(I)+.125*D(I)*R
       2-(1./120.)*D(I)*R-(1./U(I))+(.75*R/U(I))-(.1*R**3/U(I))))
27      CONTINUE
22      URK=U(1)+(1./6.)*(RK(1)+2.*RK(2)+2.*RK(3)+RK(4))*H
        IF(ICHK.EQ.0)GOTO405
        WRITE(6,406)E(4),URK
406     FORMAT(F13.8,F23.8)
405     IF(USC-URK)40,40,41
41      DO50I=1,4
        GOTO(51,52,53,54),I
51      U(1)=URK
        E(1)=E(4)
        GOTO55
52      E(2)=E(1)+H/2.
        U(2)=URK+H*RK(1)/2.
        GOTO55
53      E(3)=E(2)
        U(3)=URK+H*RK(2)/2.
        GOTO55
54      E(4)=E(1)+H
        U(4)=URK+H*RK(3)
55      D(I)=3.*(1.-(1./U(I)))
        R=D(I)/E(I)
        SC=DTA(J)
        RK(I)=U(I)*(.375-.125*R**2+.025*R**4)/((9.*(9.-(16./U(I))+
       1(7./U(I)**2))/(20.*E(I)*SC))-(.375*E(I)-(1./3.)*D(I)+.125*D(I)*R
       2-(1./120.)*D(I)*R-(1./U(I))+(.75*R/U(I))-(.1*R**3/U(I))))
50      CONTINUE
80      URK=U(1)+(1./6.)*(RK(1)+2.*RK(2)+2.*RK(3)+RK(4))*H
        IF(ICHK.EQ.0)GOTO407
        WRITE(6,406)E(4),URK
407     IF(USC-URK)40,40,41
40      VAR(J)=E(4)
        IF(J.EQ.2)GOTO69
        HOLD=URK
        CTH=E(4)
        GOTO70
69      HOLDM=URK
        CTHM=E(4)
70      CONTINUE
        DEL=VAR(1)*A
        ETA=VAR(2)*A
        IF(ICHK.EQ.0)GOTO460
        WRITE(6,461)DEL,ETA
461     FORMAT(//' ENTHALPY PL   NK = ',F10.8,' FEET, CONC BL THK = ',F10.8
       1,' FEET')
C
C       CALCULATION OF MIXED MEAN PSYCHROMETRIC CONDITIONS AT EXIT.
C
460     IX=USC*((-IW*DSTR/3.)+(IE-IW)*DSTR*((-1.*DSTP/(8.*VAR(1)))
       1+((DSTP/ VAR(1))**3/120.))+IE-(3.*(IE-IW)*VAR(1)/8.))
        CONC=USC*((-MW*DSTR/3.)+(ME-MW)*DSTR*((-1.*DSTR/(8.*VAR(2)))
       1+((DSTR/VAR(2))**3/120.))+ME-(3.*(ME-MW)*VAR(2)/8.))
        SH=1./((1./CONC)-1.)
        TDR=(IX-1060.5*SH)/(.24+.45*SH)
        IF(TDR-70.)93,94,94
93      TDR=(IX-1061.5*SH)/(.24+.439*SH)
94      SH=SH*7000.
        IF(ICHK.EQ.0)GOTO470
        WRITE(6,471)TDR,SH
        WRITE(4,219)
471     FORMAT(//////' RESULT:   DRY BULB TEMP = ',F10.5,' DEG F,  SPECIFIC
       1 HUMIDITY = ',F10.5,' LBM VAPOR/LBM DRY AIR')
        GOTO999
470     CJS=(DLOG(DABS((TEDP-TW)/(TDB-TW)))*WIDE/(2.*X(L)))*DTA(1)**0.6667
        CJI=(DLOG(DABS((IE-IW)/(IX-IW)))*WIDE/(2.*X(L)))*DTA(1)**0.66667
        CONE=SHE/(1.+SHE)
        CONW=SHW/(1.+SHW)
        CJM=(DLOG(DABS((CONE-CONW)/(CONC-CONW)))*WIDE/(2.*X(L)))*DTA(2)**0
       1.66667
```

```
      SHEX=SH/7000.
      CR=(SHE+SHEX)/(2.*SHR)
      HTCI=(DEN*UBAR*WIDE/X(L))*PLOG((IT-TW)/(IX-TW))*30.
      GAMMA=COND/CP
      ENUS=HTCI*2.*WIDE/(12.*GAMMA)
      WRITE(6,352)X(L),XSTR,TDB,SH,CR,CJT,CJM,CJS,ENUS
352   FORMAT(2X,F8.5,2X,F8.6,1X,F8.2,3X,F8.4,1X,F8.4,3X,F8.6,2X,F8.6,2X,
     1F8.6,1X,F8.3)
999   CONTINUE
      WRITE(6,217)
      WRITE(6,218)
      WRITE(6,518)
200   FORMAT(1H1'     PASSAGE DATA AND DIMENSIONS'//)
201   FORMAT(' PASSAGE WIDTH = ',F6.4,' INCHES')
202   FORMAT( ' PASSAGE HEIGHT = ',F9.4,' INCHES')
204   FORMAT( ' FLOW RATE = ',F9.2,' CFM')
205   FORMAT( ///'     PHYSICAL DATA'//)
206   FORMAT(' PRANDTL NUMBER = ',F6.4,2X,'SCHMIDT NUMBER = ',F6.4)
207   FORMAT(' SPECIFIC HEAT = ',F6.4,' BTU/LBM-F',2X,' THERMAL CONDUCTI
     1VITY = ',F6.4,' BTU/HR-FT-F')
208   FORMAT( ' KINEMATIC VISCOSITY = ',F6.4,' SQ.FT./HR')
209   FORMAT( ///'     AIR AND EXCHANGER CONDITIONS'//)
210   FORMAT(' WET BULB TEMPERATURE AT ENTRANCE = ',F6.2,' DEGREES F')
211   FORMAT( ' DRY BULB TEMPERATURE AT ENTRANCE = ',F6.2,' DEGREES F')
212   FORMAT( ' WALL TEMPERATURE = ',F6.2,' DEGREES F')
214   FORMAT( ///'     CALCULATED CONDITION OF AIR AT SELECTED POINTS'/
     1/)
217   FORMAT( /'   (THE ABOVE CALCULATIONS ASSUME THAT THE AIR IS')
218   FORMAT('  COMPLETELY MIXED AT EACH STATION AS IF THAT STATION')
219   FORMAT(1H1)
518   FORMAT('   ALONE WERE THE EXIT)')
300   CONTINUE
      GOTO234
535   STOP
      END
```

APPENDIX C

TEST APPARATUS

A general description and layout drawing of the apparatus used to obtain experimental data for this study is presented in Chapter IV. This appendix is devoted to a more thorough description of individual items of equipment.

Loop Description

Figure 19 (which is found at the end of this appendix) shows the actual device presented schematically in Figure 12. The apparatus is of the closed loop type which makes for more rapid stabilization of psychrometric properties. In heating operation, it is necessary to open the loop since there is no provision for the secondary cooling necessary to stabilize operation. This is accomplished by removing the ductwork at the inlet to the blower and replacing it with a section of duct that directs the air out of the room. While this operation requires more time for stabilization and is more directly dependent upon room conditions, it is nevertheless satisfactory.

The ductwork consists of four-inch schedule 40 stainless steel pipe in the vicinity of the blower discharge and six-inch diameter commercial circular sheet metal duct

between the main humidifier and the flow-straightening section. Specially fabricated four-inch by six-inch galvanized steel ductwork is used in the vicinity of the test section. Ductwork insulation consists of one inch of fiberglass batting with a vinyl vapor shield. It is applied in three-foot sections and held in place with elastic bands to facilitate removal.

Blower

Air is supplied by a Spencer three-stage centrifugal blower capable of a maximum pressure of sixteen inches of water and 200 cfm at eight inches of water (which is approximately the maximum flow rate possible with the loop assembled). It is powered by an 1800 rpm direct-drive 220-440 volt, three phase, three horsepower motor. Flow control is accomplished by a four-inch butterfly valve on the discharge side.

Heater

A special heater was constructed and installed downstream of the flow control valve. It consists of a six-inch diameter body 13 inches long. Nichrome ribbon is mounted on ceramic insulators forming a series connection which crosses the flow path. Total heater resistance is 7.062 ohms as measured by a Wheatstone bridge. Power is supplied by a 220-volt motor-driven autotransformer. A voltmeter and an ammeter in the heater circuit measure power input.

Humidifier

Humidification can be accomplished with two different systems depending upon the humidity range desired. For low humidities or low flow rates, a mechanical humidifier installed in the inlet to the blower can be used. This system has the advantages of relatively precise control and low temperature operation. For most runs, however, a steam system is used either exclusively or in conjunction with the mechanical humidifier. Five psig steam is throttled through a Wallace and Tiernan rotometer and introduced to the flow by a one-fourth inch diameter sparger located downstream from the heater in a vertical section of the duct. A tee below the humidifier provides a means for removal of excess moisture often encountered during startup. A constant condensate bleed ahead of the throttling needle valve prevents any liquid from being introduced during operation.

Test Section

A Harrison oil cooler was modified to approximate the mathematical model discussed in Chapter III. A jig was constructed to hold the exchanger "on end" and acryllic resin was poured into the airspace. In seeking its own level, the resin formed a wall parallel to the path of the air. This procedure was repeated on the other end resulting in an exchanger of 13 air passages, each of one-eighth inch by six inch flow area. Plate length in the flow direction is three

inches. The exchanger was mounted in a plywood case with one-half-inch Plexiglass on two sides to facilitate observation of condensate deposition.

The exchanger is attached to two four-inch by six-inch sections of galvanized steel duct. The upstream section is approximately four feet long. Adjustable baffles at the entrance to this duct combined with five aluminum "honeycomb" straighteners (three-fourths-inch thick with approximately one-sixteenth-inch diameter passages) are used to straighten and flatten the velocity profile. The downstream portion of the duct is approximately two and one-half feet long and is terminated with a rectangular tee. The main body of the flow passes through two sets of baffles which remove condensate droplets. These droplets are collected in a funnel on the lower branch of the tee and are drained continuously. The air emerges from the baffles at right angles to the original flow.

Pitot Section

A pitot-static tube is used to make measurements of flow rate in the loop. In order to produce impact pressures sufficiently high to be read reliably on a micromanometer, a section of two-inch schedule 40 galvanized steel pipe approximately three feet long is located upstream from the blower. Aluminum honeycomb straighteners separate the tube from the blower to minimize swirl in the vicinity of the measurement. The pitot tube is mounted in a ferrule fitting

which allows the cross-section to be traversed. In actual operation, only the centerline impact pressure is measured and correlated to bulk velocity as recommended in the ASHRAE Handbook of Fundamentals.

Temperature Measurement

All temperature data used in calculations are measured with 24-gage copper-constantan thermocouples and recorded on a Leeds and Northrup roll-type pen recorder. Each thermocouple is attached to an external 12-point switch at the recorder. A cold junction is maintained by an ice-water mixture in a 12-inch Dewar flask. The thermocouple junctions are submerged in a glycerine-filled test tube which minimizes fluctuations in cold junction temperature during ice renewal. A Leeds and Northrup potentiometer is attached to the last point on the switch which allows on-line calibration of the recorder.

Thermocouples used to measure ordinary thermodynamic temperatures are mounted on one-fourth-inch stainless steel tubes using room-temperature-curing silicone sealant. Ferrule fittings are used to position the probes. Wet bulb temperatures are measured by attaching thermocouples to the bulbs of liquid-in-glass thermometers.[1] A cotton wick is

---

[1]This system is used since fine-gage thermocouple wire can occasionally work through the wicking material and no longer be subjected to adiabatic saturation temperature. An occasional comparison of thermocouple and thermometer readings provides a convenient check.

slipped over the bulb and submerged in a small reservoir of water. The reservoir is attached to clear plastic tubing outside the duct to facilitate observation and addition of water. The filler tube is reattached to the duct during operation to balance blower pressure. Measurement is made downstream of orifice plates sized to provide the 1500 feet per minute minimum velocity recommended in the ASHRAE Handbook of Fundamentals. Three different orifice sizes are used in order to provide the necessary velocity at low flow rates without unnecessarily restricting the flow at higher velocities.

Pressure Measurement

Primary pressure measurements include the following:

1. Static pressure upstream from the exchanger
2. Pressure drop across the exchanger
3. Static pressure in the pitot section
4. Pitot-static head

Items (1) and (3) are used for density calculations and, while important. do not seriously affect the accuracy of the calculations due to the pressure characteristics of the blower. Therefore, these measurements are monitored continuously with two 16-inch vertical water manometers.

Items (2) and (4) are both smaller and more critical to accurate results than items (1) and (3). Thus, a more sophisticated micromanometer is used. This device operates on

the same principle as the simpler water column manometer. However, direct observation of the top of the water column is replaced by an optical system that allows accurate determination of the top of the main reservoir. A fine screw calibrated with a vernier is used to provide a liquid head that balances the measured pressure thereby returning the reservoir to some pre-determined level. The least count of this instrument is 0.0005 inches of liquid. A single instrument is used to make both pressure drop and pitot-static readings. Two three-way valves are used to switch systems.

Static pressure taps are located approximately two feet (five diameters) upstream and three feet (seven diameters) downstream from the test exchanger. The taps were constructed by soldering one-fourth-inch brass ferrule fittings on the outside of the duct and drilling through the duct wall. The edges of the taps were smoothed by hand. Instrument connections are made by one-fourth-inch polypropylene tubing and plastic ferrule fittings.

Refrigeration System

Preliminary calculations indicated that the test exchanger, maintained at about $40^{\circ}F$, would require about one quarter of a ton of refrigeration. Using chilled water as the means of energy exchange, further calculations showed that approximately 10 gallons per minute at $35^{\circ}F$ would produce the desired wall temperature.

The device, shown in Figure 20, designed to accomplish

this consists of a 110-volt, three-fourth-ton capacity hermetically sealed Refrigerant 12 compressor, single-row condenser and evaporator coils and a 110-volt, one-fourth-horsepower 18 gallon per minute centrifugal pump. The condenser coil is mounted vertically in a three-inch by eighteen-inch by eighteen-inch sheet metal container. Tap water is introduced at the bottom and overflowed above the top of the coil. A capillary tube is attached at the outlet of the condenser. The evaporator coil is mounted horizontally in an 18-inch by 18-inch by 12-inch reservoir insulated with one inch of fiberglass. The bottom outlet of this reservoir is attached to the inlet of the pump. After circulating water through the test exchanger, the pump returns it to the top of the evaporator reservoir and sprays it over the coil. All referigerant connections are made with stainless steel AN shoulder fittings. Coil joints are made with soft solder. Water connections are made with flexible hoses and aluminum AN fittings.

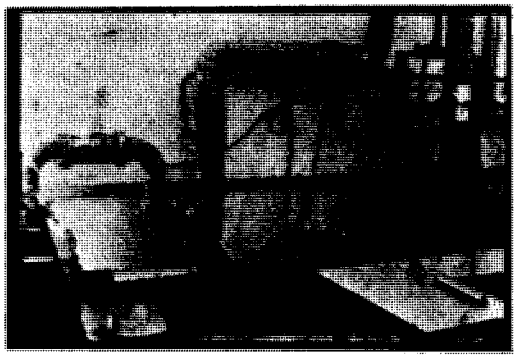

Figure 19. Actual Experimental Dehumidifying Loop

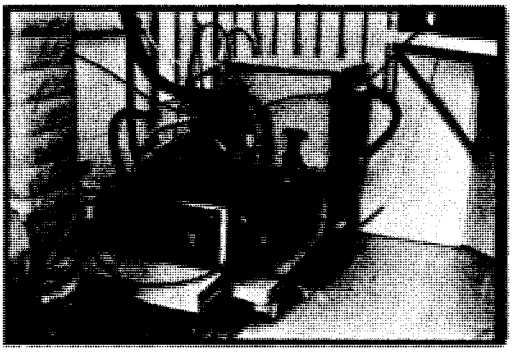

Figure 20. Water Chiller

APPENDIX D

DATA REDUCTION

Reduction of wet test data is accomplished with the computer program shown in Table II. This description will follow the chronology of that program. The dry test data reduction program is shown in Table III.

Input Data

In addition to the obvious geometrical parameters which do not change during the tests, experimental data indicated in Table II is required. Since it is most convenient to obtain temperatures directly from the recorder (which provides output in "percent of scale"), the upper and lower scale limits (E_U and E_L) are read as input and the corresponding thermocouple emf readings calculated by

$$E = E_L + \left[\frac{E_U - E_L}{100}\right] \times \text{scale reading}$$

The corresponding temperature is then calculated from a least squares curve fit of thermocouple output

$$t = 32.045 + 46.573\ E - 1.161\ E^2$$

which is accurate within 0.1% of the published data for

copper-constantan (within the limitations of instrumentation, a hypsometer used in conjunction with an ice-water cold junction showed that the thermocouple wire performed according to the published nominal predictions).

Property Calculation

Properties at each point are computed in essentially the same fashion as described for analytical calculations in Appendix B. A slight correction for the specific heat of air (given in reference [39], page 152)

$$C_p = 0.2407 + 0.2062\,\omega \qquad (\text{BTU/lbm-}^{\circ}\text{F})$$

is incorporated.

Flow Rate Calculation

Pitot-static probe traverses of the pitot section over the complete range of flow rates established that the mean reading is related to the centerline reading by

$$P_m = 0.922\,\Delta P_{\ell}$$

in accordance with specifications of F.W. Dwyer Manufacturing Company Bulletin H-11. The velocity is given by the equation

$$V = 1096.2\sqrt{\frac{0.922\,\Delta P_{\ell}}{\rho_{air}}} \qquad (\text{ft/min})$$

Wall Temperature Check

Since direct wall temperature measurements are subject to error due to improper placement of the thermocouple, an energy balance on the water passing through the exchanger is used to calculate the wall temperature. Estimating the free area of the water passage at about 50% (due to the presence of baffles), the velocity (and therefore the Reynolds number) of the water is calculated by the continuity equation. Since this configuration is approximated by Figure 10-71, page 218, of "Compact Heat Exchangers" by Kays and London [29], the j-factor is estimated to be

$$j = \exp\left[-0.3 \ln(Re) - 2.3\right]$$

which makes possible the calculation of the surface heat transfer coefficient. The overall inside film coefficient between the water and the air surface of the exchanger is therefore

$$U = \frac{1}{\frac{1}{h} + \frac{1/32}{200}}$$

where the second factor in the denominator represents the thermal resistance of the stainless steel walls. Equating the enthalpy change of the air to the convective heat transferred through the walls to the cooling water,

$$\left[\dot{M}\Delta i\right]_{air} = U(t_w - t_a)A$$

where t_a is the average temperature of the water passing through the exchanger and A is the total heat transfer area. The wall temperature t_w calculated by this method is, on the average, less than one-half degree different from the mean measured wall temperature.[1]

J-Factor Calculation

These calculations are identical to those described in Appendix B for analytical computations. The Prandtl number is calculated by the relation

$$Pr^{2/3} = 0.803014 - 1.1057 \times 10^{-4}\, t(db) + 6.88933 \times 10^{-8}\, t(db)^2$$

as suggested in reference [39], page 153.

Friction Factor Calculation

The Fanning friction factor is calculated according to Chapters 2 and 5 of "Compact Heat Exchangers" by Kays and London [29]. For cores of the type tested, it is common practice to define the friction factor so as to account for pressure drop due exclusively to viscous shear. Thus, the

---

[1] Ideally, the heat absorbed by the cooling water could be calculated by means of the measured difference in the temperature of the chilled water at the inlet and outlet. However, since the flow rate of water is kept high in an effort to approximate the constant wall temperature condition, minor errors in measuring water temperatures could result in very large errors in temperature difference.

relation

$$\Delta P = \frac{G^2}{2g_c} v_1 \left[(K_c + 1 - \sigma^2) + 2\left(\frac{v_2}{v_1} - 1\right) + f\frac{A}{A_c}\frac{v_m}{v_1} - (1 - \sigma^2 - K_e)\frac{v_2}{v_1} \right]$$

is used to define the friction factor. The terms in the brackets on the right are, respectively, entrance effect, flow acceleration, core friction and exit effect. The factors K_e and K_c are functions of flow conditions and geometry and are ordinarily obtained graphically. However, in order to facilitate machine calculations, polynomial approximations to these factors were computed. Below a Reynolds number of 2000,

$$K_e = 0.998 - 2.387\sigma + 0.992\sigma^2$$

and

$$K_c = 0.796 + 0.051\sigma - 0.445\sigma^2$$

For a Reynolds number of 2000,

$$K_e = 1.004 - 2.088\sigma + 1.002\sigma^2$$

and

$$K_c = 0.497 - 0.002\sigma - 0.406\sigma^2$$

For a Reynolds number of 10000,

$$K_c = 0.468 - 0.012\sigma - 0.388\sigma^2$$

K_e is not a particularly strong function of the Reynolds number in the range of σ considered here and is thus taken to be the same as for Re = 2000. Values of K_c for Reynolds numbers between 2000 and 10000 are obtained by linear interpolation.

Since actual pressure measurements are made several feet from the test exchanger in order to prevent the disturbance caused by the core from affecting static pressure measurements, a small correction for loss in the duct is subtracted from the experimental pressure drop reading. For five feet of four-inch by six-inch duct in the 10 to 200 cubic feet per minute range

$$\Delta P = \left[4.301 \times 10^{-4} \text{ (cfm)} + 1.293 \times 10^{-5} \text{ (cfm)}^2 - 3.86 \times 10^{-3}\right]\frac{5}{100} \qquad \text{(inches of water)}$$

according to a curve fit of data taken from a Trane duct pressure drop calculator. This is merely a first order approximation to the proper correction but is considered adequate since the correction is generally about two orders of magnitude smaller than the actual reading.

Energy and Mass Balance

As a final check on the accuracy of measurements, an order-of-magnitude analysis of energy and mass flow in the system is made. The mass balance consists of collecting all condensate removed from the air over a measured time interval. This average flow rate is compared to

$$\dot{M}_{H_2O} = (m_{in} - m_{out})\dot{M}_{air}$$

Energy input to the loop from three sources is considered. The heater input is calculated by the relation

$$Q_h = 3.413(\text{volts})(\text{amps})$$

assuming totally resistive heating. Input from latent sources (humidification) is calculated by

$$Q_L = 1060\ \dot{M}_{H_2O}$$

The energy input from the blower was determined by tests on the loop prior to the installation of the refrigeration system. By eliminating latent and sensible contributions and allowing the loop to operate open, temperature measurements over a period of time established that the energy input from the blower is related to the flow rate by

$$Q_b = 1101.2 - 5.126\ (\text{cfm}) + 5.946 \times 10^{-2}\ (\text{cfm})^2$$

These three contributions are compared to

$$Q_{removed} = (\Delta i)\ \dot{M}_{air}$$

Large differences in the energy input and energy removal indicate instrument malfunction or non-steady state operation.

TABLE II

COMPUTER PROGRAM FOR REDUCTION OF WET TEST DATA


```
C
C                    DATA REDUCTION FOR EXPERIMENTAL DEHUMIDIFYING LOOP
C
C                              INSTRUCTIONS FOR DATA INPUT
C
C
C     CARD#1 (PRINT OPTION) FOR COMPLETE RECORD OF CALCULATIONS,  PLACE
C        '0.0' ON THIS CARD.  FOR LESS DETAIL, PLACE '1.0'. (F10.5)
C
C     CARD #2 (TEMPERATURE RECORDER SCALE FACTORS) LOWER AND UPPER
C        LIMITS (IN MV) REPRESENTED BY '0%' AND '100%' ON THE RECORDER
C        (2F10.5)
C
C     CARD #3 (THERMOCOUPLE CONSTANTS) CONSTANTS A,B AND C OF EQUATION
C              T = A + B*(MV) + C*(MV)**2
C        (3F10.5)
C
C     CARD #4 (SCHMIDT NUMBER) F10.5
C
C     CARD #5 (DIMENSIONS) DISTANCE BETWEEN PLATES (INCHES),LONGEST DUCT
C        SIDE (INCHES), LENGTH OF PLATES PARALLEL TO FLOW DIRECTION
C        (INCHES), SHORTEST DUCT SIDE (INCHES), NUMBER OF PASSAGES,
C        CROSS-SECTIONAL AREA OF PITOT SECTION (SQ FT)  (6F10.5)
C
C     CARD #6 (TEMPERATURE RECORDER READINGS, % OF SCALE) TDB (A),
C        TWB(A), TDB(B), TDB(C), TDB(D), TWB(D), WATER IN, WATER OUT,
C        WALL IN, WALL OUT (10F5.1)
C
C     CARD #7 (PRESSURE DATA, INCHES OF WATER) PRESSURE DROP ACROSS
C        EXCHANGER, STATIC PRESSURE UPSTREAM FROM EXCHANGER, STATIC
C        PRESSURE AT PITOT SECTION, PITOT STATIC PRESSURE, ATMOSPHERIC
C        PRESSURE (INCHES OF MERCURY)  (5F10.5)
C
C     CARD #8 (ENERGY AND MASS BALANCE) HEATER VOLTAGE (VOLTS),
C        HEATER CURRENT (AMPS), CONDENSATE COLLECTED (CC), TIME FOR
C        CONDENSATE COLLECTION (MIN)  (4F10.5)
C
C     CARD #9 (IDENTIFICATION) RUN NUMBER, DAY, MONTH, YEAR  (4F10.5)
C
C
C
C     CARD NUMBERS 6 THROUGH 9 ABOVE MAY BE REPEATED AS OFTEN AS
C     DESIRED.  A BLANK CARD AT THE END OF THE DATA WILL PROPERLY
C     SPACE THE OUTPUT.
C
C
      DIMENSION C(10),T(10),PSWB(6)
      READ(5,504)CHK
      ICHK=CHK+0.001
      IF(ICHK.EQ.0)GOTO963
      WRITE(6,800)
      WRITE(6,801)
800   FORMAT(1H1,/////,'  REYNOLDS          DRY BULB TEMPS (F)          WE
     1T BULB TEMPS (F)    WALL     PRESS DROP     TOTAL      MASS     SENSIB
     2LE     FANNING')
801   FORMAT('   NUMBER      T(A)     T(B)     T(C)     T(D)        T(A)    T
     1(D)     TEMP (F)  (IN WATER)  J-FACTOR  J-FACTOR  J-FACTOR  FRIC F
     2ACTOR')
963   READ(5,502)BOT,TOP
502   FORMAT(2F10.5)
      READ(5,503)TC1,TC2,TC3
503   FORMAT(3F10.5)
      READ(5,504)SF
504   FORMAT( F10.5)
      READ(5,505)   GAP,FLG,DEPTH,WIDTH,FN,APIT
505   FORMAT(6F10.5)
200   READ(5,500)(C(I),I=1,10)
500   FORMAT(10F5.1)
      IF(C(1).EQ.0.0)GOTO201
      READ(5,501)DP,P1,P3,VP,ATMPR
      READ(5,501)VOLTS,AMPS,CCH,TIME
      READ(5,501)RUN,DAY,EMO,YR
      IRUN=RUN+.0001
      IDAY=DAY+.0001
      MO=EMO+.0001
      IYR=YR+.0001
501   FORMAT(5F10.5)
C
C        CALCULATION OF TEMPERATURES FROM CHART READINGS
C
      DO50I=1,10
      EMF=((TOP-BOT)/100.)*C(I)+BOT
50    T(I)=TC1+TC2*EMF+TC3*EMF**2
C
C        CALCULATION OF SPECIFIC HUMIDITIES, ENTHALPIES AND DENSITIES
C
      TK=((T(2)-32.)/1.8)+273.16
      XX=647.27-TK
      Y=XX*(3.244+(5.86E-03+1.17E-08*XX**2)*XX)/(TK*(1.+2.188E-03*XX))
      PSWB(2)=14.696*21**.167/(10.**Y)
      VPA=PSWB(2)-((14.696-PSWB(2))*(T(1)-T(2))/(2800.-1.3*T(2)))
      SHA=0.622*(VPA/(14.696-VPA))
      IF(T(3).GT.70.0)GOTO300
      H3=(10.2062*SHA+.2407)*T(3)+SHA*(1061.7+.439*T(3)))/(1.+SHA)
      GOTO301
300   H3=((.2062*SHA+.2407)*T(3)+SHA*(1060.5+.45*T(3)))/(1.+SHA)
301   TK=((T(6)-32.)/1.8)+273.16
      XX=647.27-TK
      Y=XX*(3.244+(5.86E-03+1.17E-08*XX**2)*XX)/(TK*(1.+2.188E-03*XX))
      PSWB(6)=14.696*218.167/(10.**Y)
      VPD=PSWB(6)-((14.696-PSWB(6))*(T(5)-T(6))/(2800.-1.3*T(6)))
      SHD=0.622*(VPD/(14.696-VPD))
      IF(T(4).GT.70.0)GOTO302
      H4=((.2062*SHD+.2407)*T(4)+SHD*(1061.7+.439*T(4)))/(1.+SHD)
      GOTO303
302   H4=((.2062*SHD+.2407)*T(4)+SHD*(1060.5+.45*T(4)))/(1.+SHD)
303   TM=(T(9)+T(10))/2.
      DENA=0.09734*((1.+SHA)/(1.+1.607*SHA))*(P1+13.55*ATMPR)/(T(3)+460.
     1)
      DENC=0.09734*((1.+SHD)/(1.+1.607*SHD))*(P1-DP+13.55*ATMPR)/(T(4)+
     1460.)
      DENE=0.09734*((1.+SHD)/(1.+1.607*SHD))*(P3+13.55*ATMPR)/(T(5)+
     1460.)
C
C        CALCULATION OF DIAMETER REYNOLDS NUMBER
C
      EPN=139.6*SQRT(0.022*VP*62.4/DENE)
      FLOW=DENE*APIT*EPN
      DH=GAP/6.
```

```
      REXVEL=FLOAT((10.*R+DENC)*FN*GAP*FLG/288.)
      CFM=REXVEL*GAP*FLG/144.
      TMM=(T(2)+T(4))/2.
      VISC=(.0393742+.00474E-5*TMM-2.653E5E-8*TMM**2)/60.
      RE=(REXVEL*EM*(EQUR+DENC)/2.)/VISC
C
C        CHECK OF WALL TEMPERATURE MEASUREMENT BY HEAT BALANCE ON WATER
C
      FLOWW=10.*6.338
      VW=FLOWW*2*5.*32./(62.4*0.*(FN+1.)*DEPTH)
      RE=4.*0.05*VW/(12.*61.*1.2E-5)
      WJ=EXP(-0.3*ALOG(REW)-2.3)
      H=60.*WJ*VW*62.4*10**0.66667
      U=1./((1./H )       +(1./(32.*200.)))
      Q=(H2-H4)*FLOWT*60.
      A=2.*FN*DEPTH*FLG/144.
      TWW=(T(7)+T(8))/2.
      TWC=TMW+(Q/(U*A))
      IF(ABS(TM-TWC).GT.2.0)TM=TWC
C
C        CALCULATION OF SENSIBLE J-FACTOR
C
      VAR1= ALOG((T(3)-TM  )/(T(4)-TM  ))*GAP/(2.*DEPTH)
      CJS=VAR1*(0.803014-1.1057E-4*((T(3)+T(4))/2.)+6.88933E-8*
     1((T(3)+T(4))/2.))
C
C        CALCULATION OF MASS J-FACTOR
C
      TK=((TM  -32.)/1.8)+273.16
      XX=647.27-TK
      Y=XX*(3.244+(5.868E-03+1.17E-08*XX**2)*XX)/(TK*(1.+2.188E-03*XX))
      PSWBM  =14.696*210.157/(10.**Y)
      SHW=0.622*(PSWBM/(14.696-PSWBM))
      PHI=(SHA+SHD)/(2.*SHW)
      CONCA=SHA/(1.+SHA)
      CONCD=SHD/(1.+SHD)
      CONCW=SHW/(1.+SHW)
      VAR2=ALOG((CONCA-CONCW)/(CONCD-CONCW))*GAP/(2.*DEPTH)
      CJM=VAR2*SC**0.66667
C
C        CALCULATION OF SENSIBLE + LATENT J-FACTOR
C
      HW=(1.2052*SHW+.2407)*TM*SHW*(1061.7+.439*TM))/(1.+SHW)
      VAR3=ALOG((H3-HW)/(H4-HW))*GAP/(2.*DEPTH)
      CJT=VAR3*(.803014-1.1057E-4*((T(3)+T(4))/2.)+6.88933E-8*
     1((T(3)+T(4))/2.))
C
C        CALCULATION OF FANNING FRICTION FACTOR
C
      SIGMA=FN*GAP/WIDTH
      IF(RE.LT.2000.)GOTO60
      FKE=1.00399-2.08779*SIGMA+1.00233*SIGMA**2
      FKC1=0.49734-0.30168*SIGMA-0.40559*SIGMA**2
      FKC2=0.46759-0.01230*SIGMA-0.33795*SIGMA**2
      FKC=FKC1-((RE-2000.)/10000. )*(FKC1-FKC2)
      GOTO61
60    FKE=0.99852-1.3973C*SIGMA+0.9914*SIGMA**2
      FKC=0.79580+0.05055*SIGMA-0.44464*SIGMA**2
61    CONTINUE
      SPV1=1./DENA
```



```
      SPV2=1./DEN
      SPVM=(SPV1+SPV2)/2.
      G=FLOWT*60.*144./(FN*FLG*GAP)
C
C                CORRECTION FOR DUCT LOSS
      DPC=DP*(1-0.0038616+0.00043011*(CFMP*FN)+0.000012933*(CFMP*FN)**2)
     1*0.02
C
      F=(((DPC*2.4/12.)*(64.4*3600**2/G**2)/SPV1)-(FKC +1.-SIGMA**2)
     1-2.*((SPV2/SPV1)-1.)+(1.-FKE-SIGMA**2)*(SPV2/SPV1))*
     1(SPV1*FN*GAP/(SPVM*2.*FN*DEPTH))
C
C        COMPARISON OF ENERGY AND MASS BALANCES BY THERMOCOUPLE
C        READINGS AND DIRECT MEASUREMENT
C
      FMOIA=CCA*62.4*60./(1728.*TIME*2.54**3)
      FMINO=(CONCA-CONCC)*FLOWT*60.
      QHTR=VOLTS*AMPS*3.413
      QPIR=1101.2-5.124*CFMP*FN+0.05946*(CFMP*FN)**2
      QLAT=FMINO*1060.
      QMTR=QHTR+QPLE+QLAT
      QINO=(H2-H4)*FLOWT*60.
      IF(ICHK.EQ.1)GOTO70
      WRITE(6,900)
900   FORMAT(1H1)
      WRITE(6,901)
901   FORMAT(////' PHYSICAL DIMENSIONS'//)
      WRITE(6,902)GAP
902   FORMAT(' DISTANCE BETWEEN PLATES = ',F8.6,' INCHES')
      WRITE(6,903)FLG
903   FORMAT(' PLATE LENGTH = ',F8.4,' INCHES')
      WRITE(6,904)DEPTH
904   FORMAT(' EXCHANGER DEPTH = ',F8.4,' INCHES')
      N=FN+.0001
      WRITE(6,905)N
905   FORMAT(' NUMBER OF PASSAGES IN EXCHANGER = ',I3)
      WRITE(6,910)
910   FORMAT(//////' EXPERIMENTAL DATA'//)
      WRITE(6,911)DP
911   FORMAT(' CORE PRESSURE DROP = ',F6.4,' INCHES OF WATER')
      WRITE(6,912)P1
912   FORMAT(' PRESSURE UPSTREAM FROM EXCHANGER = ',F7.4,' INCHES OF WAT
     1ER')
      WRITE(6,913)P2
913   FORMAT(' PITOT SECTION PRESSURE = ',F7.4,' INCHES OF WATER')
      WRITE(6,914)VP
914   FORMAT(' CENTERLINE PITOT-STATIC READING = ',F6.4,' INCHES OF WATE
     1R')
      WRITE(6,995)AMPS,VOLTS
995   FORMAT(' HEATER INPUT = ',F6.2,' AMPS AT ',F6.2,' VOLTS')
      WRITE(6,996)CCA,TIME
996   FORMAT(' CONDENSATE COLLECTION = ',F6.2,' CC IN ',F6.2,' MINUTES')
      WRITE(6,915)T(1)
915   FORMAT(' DRY BULB TEMPERATURE AT A-SECTION = ',F7.2,' DEGREES F')
      WRITE(6,916)T(2)
916   FORMAT(' WET BULB TEMPERATURE AT A-SECTION = ',F7.2,' DEGREES F')
      WRITE(6,917)T(3)
917   FORMAT(' DRY BULB TEMPERATURE AT B-SECTION = ',F7.2,' DEGREES F')
      WRITE(6,918)T(4)
918   FORMAT(' DRY BULB TEMPERATURE AT C-SECTION = ',F7.2,' DEGREES F')
```

```
      WRITE(6,919)T(6)
  919 FORMAT(' DRY BULB TEMPERATURE AT D-SECTION = ',F7.2,' DEGREES F')
      WRITE(6,920)T(8)
  920 FORMAT(' WET BULB TEMPERATURE AT D-SECTION = ',F7.2,' DEGREES F')
      TAVW=(T(7)+T(8))/2.
      WRITE(6,921)TAVW
  921 FORMAT(' AVERAGE COOLING WATER TEMPERATURE = ',F7.2,' DEGREES F')
      TAVS=(T(9)+T(10))/2.
      DN=(T(10)-T(9))/2.
      WRITE(6,922)TAVS
  922 FORMAT(' AVERAGE MEASURED WALL TEMPERATURE = ',F7.2,' DEGREES F  (
     1+')
      WRITE(6,923)DN
  923 FORMAT('+',66X,'- ',F7.5,' DEGREES F)')
      WRITE(6,924)
  924 FORMAT(////' CALCULATED DATA'//)
      WRITE(6,925)FLOAT
  925 FORMAT(' MASS FLOW RATE = ',F7.3,' LBM/MIN')
      WRITE(6,991)CFMP
  991 FORMAT(' VOLUME FLOW RATE PER PASSAGE = ',F6.3,' CUBIC FEET/MIN')
      WRITE(6,926)RE
  926 FORMAT(' REYNOLDS NUMBER = ',F8.2)
      WRITE(6,927)EXVEL
  927 FORMAT(' PASSAGE VELOCITY =',F8.2,' FEET/MIN')
      WRITE(6,994)H
  994 FORMAT(' WATER-SIDE SURFACE COEFFICIENT = ',F7.2,' BTU/HR-SQ FT-DE
     1G F')
      WRITE(6,993)TWC
  993 FORMAT(' AVERAGE WALL TEMPERATURE (CALCULATED) = ',F7.2,' DEGREES
     1F')
      WRITE(6,932)TM
  932 FORMAT(' WALL TEMPERATURE USED IN CALCULATIONS = ',F7.2,' DEGREES
     1F')
      WRITE(6,980)QQIR
  980 FORMAT(' APPROXIMATE ENERGY INPUT TO LOOP = ',F8.2,' BTU/HR')
      WRITE(6,981)QIND
  981 FORMAT(' ENERGY REMOVAL FROM AIR = ',F8.2,' BTU/HR')
      WRITE(6,982)EMDIR
  982 FORMAT(' APPROXIMATE CONDENSATE REMOVAL FROM LOOP = ',F8.6,' LBM/H
     1R')
      WRITE(6,983)EMIND
  983 FORMAT(' CHANGE IN MOISTURE CONTENT OF AIR CROSSING EXCHANGER = ',
     1F8.6,' LBM/HR')
      WRITE(6,941)
  941 FORMAT(' CONCENTRATION RATIO (O')
      WRITE(6,942)PHI
  942 FORMAT('+',21X,'/) = ',F7.3)
      WRITE(6,928)CJS
  928 FORMAT(' SENSIBLE HEAT TRANSFER J-FACTOR = ',F7.5)
      WRITE(6,992)CJI
  992 FORMAT(' TOTAL (SENSIBLE PLUS LATENT) HEAT TRANSFER J-FACTOR = ',F
     17.5)
      WRITE(6,929)CJM
  929 FORMAT(' MASS TRANSFER J-FACTOR = ',F7.5)
      HTCI=CJI*6./.7**.66667
      ENUS=HTCI*DH/(     .015/.24)
      WRITE(6,600)ENUS
  600 FORMAT(' NUSSELT NUMBER = ',F7.3)
      WRITE(6,930)F
  930 FORMAT(' FANNING FRICTION FACTOR = ',F7.5)
```



```
      WRITE(6,941)RUN,MO,IDAY,IYR
  941 FORMAT(100X,'RUN NUMBER',I2,5X,I2,'/',I2,'/',I2)
      GOTO230
   70 WRITE(6,71)EE,T(1),T(3),T(4),T(5),T(2),T(6),TM,DP,CJI,CJM,CJS,F
   71 FORMAT(2X,F7.0,1X,4F8.2,3X,2F8.2,3X,F8.2,4X,F8.4,4X,F8.5,2X,F8.5,2
     1X,F8.5,3X,F8.5)
      GOTO200
  201 WRITE(6,900)
      STOP
      END
```

TABLE III

COMPUTER PROGRAM FOR REDUCTION OF DRY TEST DATA

1/4

```
C
C                    DATA REDUCTION FOR EXPERIMENTAL HEATING LOOP
C
C                          INSTRUCTIONS FOR DATA INPUT
C
C
C     CARD#1 (PRINT OPTION) FOR COMPLETE RECORD OF CALCULATIONS,  PLACE
C        '0.0' ON THIS CARD.  FOR LESS DETAIL, PLACE '1.0'. (F10.5)
C
C     CARD #2 (TEMPERATURE RECORDER SCALE FACTORS) LOWER AND UPPER
C        LIMITS (IN MV) REPRESENTED BY '0%' AND '100%' ON THE RECORDER
C        (2F10.5)
C
C     CARD #3 (THERMOCOUPLE CONSTANTS) CONSTANTS A,B AND C OF EQUATION
C           T = A + B*(MV) + C*(MV)**2
C        (3F10.5)
C
C     CARD #4 (DIMENSIONS) DISTANCE BETWEEN PLATES (INCHES),LONGEST DUCT
C        SIDE (INCHES), LENGTH OF PLATES PARALLEL TO FLOW DIRECTION
C        (INCHES), SHORTEST DUCT SIDE (INCHES), NUMBER OF PASSAGES,
C        CROSS-SECTIONAL AREA OF PITOT SECTION (SQ FT)  (6F10.5)
C
C     CARD #5 (TEMPERATURE RECORDER READINGS, % OF SCALE) TDB (A),
C        TWB(A), TDB(B), TDB(C), TDB(D), TWB(D), WATER IN, WATER OUT,
C        WALL IN, WALL OUT (10F5.1)
C
C     CARD #6 (PRESSURE DATA, INCHES OF WATER) PRESSURE DROP ACROSS
C        EXCHANGER, STATIC PRESSURE UPSTREAM FROM EXCHANGER, STATIC
C        PRESSURE AT PITOT SECTION, PITOT STATIC PRESSURE, ATMOSPHERIC
C        PRESSURE (INCHES OF MERCURY)  (5F10.5)
C
C     CARD #7 (IDENTIFICATION) RUN NUMBER, DAY, MONTH, YEAR  (4F10.5)
C
C
C
C     CARD NUMBERS 5 THROUGH 7 MAY BE REPEATED AS OFTEN AS DESIRED.
C     A BLANK CARD AT THE END OF THE DATA WILL PROPERLY SPACE THE OUTPUT.
C
C
      DIMENSION C(10),T(10),PSWB(6)
      READ(5,504)CHK
  504 FORMAT(F10.5)
      ICHK=CHK+0.001
      IF(ICHK.LT.1)GOTO963
      WRITE(6,800)
      WPITE(6,801)
  800 FORMAT(1H1,//////,'  REYNOLDS          DRY BULB TEMPS (F)          WE
     1T BULB TEMPS (F)    WALL    PRESS DROP   J-FACTOR    FANNING')
  801 FORMAT('   NUMBER      T(A)     T(B)     T(C)     T(D)      T(A)     T
     1(D)     TEMP (F)  (IN WATER)          FRIC FACTOR'/)
  963 READ(5,502)BOT,TOP
  502 FORMAT(2F10.5)
      READ(5,503)TC1,TC2,TC3
  503 FORMAT(3F10.5)
      READ(5,505)   GAP,FLG,DEPTH,WIDTH,FN,APIT
  505 FORMAT(6F10.5)
  200 READ(5,500)(C(I),I=1,10)
  500 FORMAT(10F5.1)
      IF(C(1).EQ.0.0)GOTO201
```

2/4

```
      READ(5,501)DP,P1,P3,VP,ATMPR
      READ(5,501)RUN,DAY,FMO,YR
      IRUN=RUN+.0001
      IDAY=DAY+.0001
      MO=FMO+.0001
      IYR=YR+.0001
  501 FORMAT(5F10.5)
C
C        CALCULATION OF TEMPERATURES FROM CHART READINGS
C
      DO50I=1,10
      EMF=((TOP-BOT)/100.)*C(I)+BOT
   50 T(I)=TC1+TC2*EMF+TC3*EMF**2
C
C        CALCULATION OF SPECIFIC HUMIDITIES, ENTHALPIES AND DENSITIES
C
      TK=((T(7)-32.)/1.8)+273.16
      XX=647.27-TK
      Y=XX*(3.244+(5.868E-03+1.17E-08*XX**2)*XX)/(TK*(1.+2.188E-03*XX))
      PSWB(2)=14.696*218.167/(10.**Y)
      VPA=PSWB(2)-((14.696-PSWB(2))*(T(1)-T(2))/(2800.-1.3*T(2)))
      SHA=0.622*(VPA/(14.696-VPA))
      IF(T(3).GT.70.0)GOTO300
      H3=((0.2062*SHA+.2407)*T(3)+SHA*(1061.7+.439*T(3)))/(1.+SHA)
      GOTO301
  300 H3=((.2062*SHA+.2407)*T(3)+SHA*(1060.5+.45*T(3)))/(1.+SHA)
  301 TK=((T(6)-32.)/1.8)+273.16
      XX=647.27-TK
      Y=XX*(3.244+(5.868E-03+1.17E-08*XX**2)*XX)/(TK*(1.+2.188E-03*XX))
      PSWB(6)=14.696*218.167/(10.**Y)
      VPD=PSWB(6)-((14.696-PSWB(6))*(T(5)-T(6))/(2800.-1.3*T(6)))
      SHD=0.622*(VPD/(14.696-VPD))
      IF(T(4).GT.70.)GOTO302
      H4=((.2062*SHD+.2407)*T(4)+SHD*(1061.7+.439*T(4)))/(1.+SHD)
      GOTO303
  302 H 4 =((.2062*SHD+.2407)*T(4)+SHD*(1060.5+.45*T(4)))/(1.+SHD)
  303 TM=(T(9)+T(10))/2.
      DENB=0.09734*((1.+SHA)/(1.+1.607*SHA))*(P1+13.55*ATMPR)/(T(3)+460.
     1)
      DENC=0.09734*((1.+SHD)/(1.+1.607*SHD))*(P3-DP+13.55*ATMPR)/(T(4)+
     1460.)
      DENE=0.09734*((1.+SHD)/(1.+1.607*SHD))*(P3+13.55*ATMPR)/(T(5)+
     1460.)
C
C        CALCULATION OF DIAMETER REYNOLDS NUMBER
C
      FPM=138.6*SQRT(0.922*VP*62.4/DENE)
      FLORT=DENE*APIT*FPM
      DH=GAP/6.
      EXVEL=FLORT/((DENB+DENC)*FN*GAP*FLG/288.)
      CFMP=EXVEL*GAP*FLG/144.
      TMM=(T(3)+T(4))/2.
      VISC=(0.0393742+6.79474E-5*TMM-2.65385E-8*TMM**2)/60.
      RE=(EXVEL*DH*(DENB+DENC)/2.)/VISC
C
C        CHECK OF WALL TEMPERATURE MEASUREMENT BY HEAT BALANCE ON WATER
C
      FLRTW= 5.*P.338
      VW=FLRTW*288.*32./(62.449.*(FN+1.)*DEPTH)
      REW=4.*0.09*VW/(12.*60.*1.8E-5)
```

```
      WJ=EXP(-0.3*ALOG(REW)-2.3)
      H=60.*WJ*VW*62.4/10**0.66667
      U=1./((1./H )       +(1./(32.*200.)))
      Q=(H3-H4)*FLOAT*60.
      A=2.*FN*DEPTH*FLG/144.
      TMW=(T(7)+T(8))/2.
      TWC=TMW+(Q/(U*A))
      IF(ABS(TM-TWC).GT.2.0)TM=TWC
C
C        CALCULATION OF COLBURN J-FACTOR
C
      VAR1= ALOG((T(3)-TM  )/(T(4)-TM  ))*GAP/(2.*DEPTH)
      CJS=VAR1*(0.803014-1.1057E-4*((T(3)+T(4))/2.)+6.88933E-8*
     1((T(3)+T(4))/2.))
C
C        CALCULATION OF FANNING FRICTION FACTOR
C
      SIGMA=FN*GAP/WIDTH
      IF(RE.LT.2000.)GOTO60
      FKE=1.00396-2.08779*SIGMA+1.00233*SIGMA**2
      FKC1=0.49734-3.0016*SIGMA-6.40559*SIGMA**2
      FKC2=0.46759-0.01239*SIGMA-0.38795*SIGMA**2
      FKC=FKC1-((RE-2000.)/10000. )*(FKC1-FKC2)
      GOTO61
60    FKE=0.99932-2.3870*SIGMA+0.99184*SIGMA**2
      FKC=0.79540+0.05055*SIGMA-0.44464*SIGMA**2
61    CONTINUE
      SPV1=1./DENB
      SPV2=1./DENC
      SPVM=(SPV1+SPV2)/2.
      G=FLOAT*60.*144./(FN*FLG*GAP)
C
C                  CORRECTION FOR DUCT LOSS
      DPC=DP-(-0.00386616+0.0004301)*(CFMP*FN)+0.000012933*(CFMP*FN)**2)
     1*0.07
C
      F=(((DPC*62.4/12.)*(64.4*3600**2/G**2)/SPV1)-(FKC +1.-SIGMA**2)
     1-2.*((SPV2/SPV1)-1.)+(1.-FKE-SIGMA**2)*(SPV2/SPV1))*
     1(SPV1*FN*GAP/(SPVM*2.*FN*DEPTH))
      IF(ICHK.EQ.1)GOTO90
      WRITE(6,900)
900   FORMAT(1H1)
      WRITE(6,901)
901   FORMAT(/////' PHYSICAL DIMENSIONS'//)
      WRITE(6,902)GAP
902   FORMAT(' DISTANCE BETWEEN PLATES = ',F8.6,' INCHES')
      WRITE(6,903)FLG
903   FORMAT(' PLATE LENGTH = ',F8.4,' INCHES')
      WRITE(6,904)DEPTH
904   FORMAT(' EXCHANGER DEPTH = ',F8.4,' INCHES')
      N=FN*.0001
      WRITE(6,905)N
905   FORMAT(' NUMBER OF PASSAGES IN EXCHANGER = ',I3)
      WRITE(6,910)
910   FORMAT(/////' EXPERIMENTAL DATA'//)
      WRITE(6,911)DP
911   FORMAT(' CORE PRESSURE DROP = ',F6.4,' INCHES OF WATER')
      WRITE(6,912)P1
912   FORMAT(' PRESSURE UPSTREAM FROM EXCHANGER = ',F7.4,' INCHES OF WAT
     1ER')
```



```
      WRITE(6,913)P3
913   FORMAT(' PITOT SECTION PRESSURE = ',F7.4,' INCHES OF WATER')
      WRITE(6,914)VP
914   FORMAT(' CENTERLINE PITOT-STATIC READING = ',F6.4,' INCHES OF WATE
     1R')
      WRITE(6,915)T(1)
915   FORMAT(' DRY BULB TEMPERATURE AT A-SECTION = ',F7.2,' DEGREES F')
      WRITE(6,916)T(2)
916   FORMAT(' WET BULB TEMPERATURE AT A-SECTION = ',F7.2,' DEGREES F')
      WRITE(6,917)T(3)
917   FORMAT(' DRY BULB TEMPERATURE AT B-SECTION = ',F7.2,' DEGREES F')
      WRITE(6,918)T(4)
918   FORMAT(' DRY BULB TEMPERATURE AT C-SECTION = ',F7.2,' DEGREES F')
      WRITE(6,919)T(5)
919   FORMAT(' DRY BULB TEMPERATURE AT D-SECTION = ',F7.2,' DEGREES F')
      WRITE(6,920)T(6)
920   FORMAT(' WET BULB TEMPERATURE AT D-SECTION = ',F7.2,' DEGREES F')
      TAVW=(T(7)+T(8))/2.
      WRITE(6,921)TAVW
921   FORMAT(' AVERAGE HEATING WATER TEMPERATURE = ',F7.2,' DEGREES F')
      TAVS=(T(9)+T(10))/2.
      PM=ABS((T(10)-T(9))/2.)
      WRITE(6,922)TAVS
922   FORMAT(' AVERAGE MEASURED WALL TEMPERATURE = ',F7.2,' DEGREES F  (
     1+')
      WRITE(6,923)PM
923   FORMAT('+',66X,'- ',F7.6,' DEGREES F)')
      WRITE(6,924)
924   FORMAT(//////' CALCULATED DATA'///)
      WRITE(6,925)FLORT
925   FORMAT(' MASS FLOW RATE = ',F7.3,' LBM/MIN')
      WRITE(6,991)CFMP
991   FORMAT(' VOLUME FLOW RATE PER PASSAGE = ',F6.3,' CUBIC FEET/MIN')
      WRITE(6,926)RE
926   FORMAT(' REYNOLDS NUMBER = ',F8.2)
      WRITE(6,927)EXVEL
927   FORMAT(' PASSAGE VELOCITY =',F8.2,' FEET/MIN')
      WRITE(6,994)H
994   FORMAT(' WATER-SIDE SURFACE COEFFICIENT = ',F7.2,' BTU/HR-SQ FT-DE
     1G F')
      WRITE(6,993)TWC
993   FORMAT(' AVERAGE WALL TEMPERATURE (CALCULATED) = ',F7.2,' DEGREES
     1F')
      WRITE(6,932)TM
932   FORMAT(' WALL TEMPERATURE USED IN CALCULATIONS = ',F7.2,' DEGREES
     1F')
      WRITE(6,928)CJS
928   FORMAT(' COLBURN J-FACTOR = ',F7.5)
      WRITE(6,930)F
930   FORMAT(' FANNING FRICTION FACTOR = ',F7.5)
      WRITE(6,931)IRUN,MO,IDAY,IYR
931   FORMAT(100X,'RUN NUMBER',I3,5X,I2,'/',I2,'/',I2)
      GOTO200
90    WRITE(6,701)RE,T(1),T(3),T(4),T(5),T(2),T(6),TM,DP,CJS,F
701   FORMAT(2X,F7.0,2X,4F8.2,3X,2F8.2,4X,F8.2,2X,F8.4,4X,F8.5,3X,F8.5)
      GOTO200
201   WRITE(6,900)
      STOP
      END
```

APPENDIX E

EXPERIMENTAL DATA

This appendix contains the experimental data obtained during the course of this study. All important raw data as well as selected calculated results are presented in tabular form. Table IV contains wet test data and Table V contains dry test data. The subscripts on temperature readings refer to the location of their measurement on Figure 12.

TABLE IV

WET TEST DATA

REYNOLDS NUMBER	DRY BULB TEMPS (F) T(A)	T(B)	T(C)	T(D)	WET BULB TEMPS (F) T(A)	T(D)	WALL TEMP (F)	PRESS DROP (IN WATER)	TOTAL J-FACTOR	MASS J-FACTOR	SENSIBLE J-FACTOR	FANNING FRIC FACTOR
873.	99.90	96.01	63.09	64.80	86.17	63.18	45.36	0.0564	0.01833	0.01682	0.01737	0.08431
949.	87.92	86.74	58.21	59.57	77.46	57.85	41.45	0.0602	0.01687	0.01554	0.01609	0.07857
1008.	108.12	103.42	67.93	68.65	81.52	62.01	43.71	0.0637	0.01525	0.01386	0.01491	0.06793
1080.	103.68	100.07	68.47	69.63	85.30	66.32	45.55	0.0717	0.01432	0.01266	0.01433	0.06718
1096.	98.78	95.41	62.28	64.08	69.01	53.50	38.77	0.0702	0.01478	0.01386	0.01455	0.06558
1133.	94.97	92.37	63.42	64.71	77.55	60.20	42.56	0.0808	0.01453	0.01314	0.01424	0.07103
1218.	107.10	103.42	68.74	71.51	80.20	63.18	44.30	0.0877	0.01428	0.01223	0.01461	0.06334
1271.	87.40	86.17	63.90	64.80	76.66	62.19	42.97	0.0909	0.01210	0.01078	0.01200	0.06296
1297.	98.10	94.70	62.28	63.09	73.29	57.67	41.08	0.1095	0.01388	0.01366	0.01269	0.07644
1319.	80.55	79.84	59.21	59.75	70.88	57.13	40.11	0.0932	0.01235	0.01113	0.01214	0.06126
1382.	108.04	104.70	72.58	74.44	81.17	64.44	45.27	0.1191	0.01371	0.01316	0.01285	0.06598
1498.	105.38	102.48	72.31	74.27	80.37	65.42	45.73	0.1658	0.01238	0.01075	0.01254	0.08320
1591.	85.56	84.51	60.47	64.08	65.87	55.77	42.28	0.1350	0.01280	0.00878	0.01395	0.06024
1762.	94.19	92.62	70.08	71.42	78.87	65.16	46.23	0.1455	0.01183	0.01119	0.01101	0.04618
1950.	88.27	87.22	68.56	69.90	79.05	67.22	46.51	0.1730	0.00998	0.00873	0.01015	0.04640
1964.	80.20	79.49	61.56	62.73	64.80	55.59	40.67	0.1804	0.00993	0.00819	0.01027	0.05082
2058.	98.26	96.62	74.62	74.80	77.46	63.99	46.05	0.1850	0.01157	0.01311	0.00944	0.04525
2260.	87.75	86.96	68.65	69.45	72.31	60.74	44.44	0.2276	0.01115	0.01237	0.00932	0.04801
2346.	81.25	80.81	62.73	64.08	65.69	56.86	41.17	0.2276	0.00945	0.00728	0.01009	0.04635
2462.	85.21	84.51	66.86	68.11	68.92	59.57	44.21	0.2420	0.00993	0.00943	0.00954	0.04310
2626.	85.74	84.85	67.67	67.93	69.19	59.75	43.71	0.2535	0.00922	0.00859	0.00895	0.03836
2738.	95.75	94.43	73.64	75.77	77.01	64.53	47.47	0.2990	0.01206	0.01372	0.00974	0.04033
3082.	80.64	80.37	60.47	65.69	65.25	57.85	43.94	0.3379	0.01120	0.00673	0.01309	0.03845
3316.	89.23	88.62	73.02	74.18	78.52	67.93	50.35	0.3891	0.01012	0.01011	0.00866	0.03525
3367.	83.10	82.66	67.67	68.29	68.83	59.12	45.04	0.3957	0.01061	0.01312	0.00842	0.03614
3700.	88.10	87.57	71.33	72.75	74.35	65.69	48.89	0.4570	0.00893	0.00781	0.00901	0.03281
3825.	89.84	89.15	70.44	72.13	68.47	61.38	46.28	0.3000	0.00821	0.00433	0.00949	0.01449
3883.	87.31	86.70	70.53	72.22	69.90	63.09	47.84	0.4806	0.00792	0.00543	0.00891	0.03060
4173.	81.87	81.43	69.45	70.17	72.22	65.42	49.89	0.6340	0.00743	0.00618	0.00791	0.03825
4325.	103.42	102.22	85.74	86.44	85.39	77.63	59.62	0.6150	0.00744	0.00611	0.00808	0.02895
4634.	88.45	87.92	73.47	74.98	74.00	67.13	51.31	0.6304	0.00772	0.00619	0.00831	0.02681
5004.	88.45	87.92	73.91	75.51	72.93	66.59	51.22	0.7180	0.00741	0.00587	0.00796	0.02572
5452.	87.14	86.70	73.02	73.55	73.11	67.04	52.36	0.8485	0.00695	0.00458	0.00841	0.02594

TABLE V

DRY TEST DATA

REYNOLDS NUMBER	DRY BULB TEMPS (F) T(A)	T(B)	T(C)	T(D)	WET BULB TEMPS (F) T(A)	T(D)	WALL TEMP (F)	PRESS DROP (IN WATER)	J-FACTOR	FANNING FRIC FACTOR
808.	95.80	93.06	111.99	108.93	71.69	76.62	125.79	0.0432	0.01424	0.06345
1031.	88.62	87.06	107.62	105.22	69.14	73.29	125.98	0.0456	0.01232	0.03565
1185.	90.45	88.62	106.76	104.96	68.87	72.95	125.73	0.0697	0.01107	0.04399
1457.	91.76	90.45	105.73	104.19	69.54	72.49	126.35	0.0924	0.00915	0.03650
1617.	92.02	90.58	104.83	103.80	70.48	75.15	125.98	0.1110	0.00850	0.03485
1816.	89.67	88.49	102.52	101.87	70.08	73.29	125.98	0.1292	0.00774	0.03159
2175.	91.11	89.62	101.87	101.23	69.68	73.02	124.79	0.1765	0.00692	0.03303
2216.	93.32	92.64	104.06	103.55	74.49	77.55	125.23	0.1885	0.00717	0.03330
2368.	89.80	89.02	101.23	100.46	69.41	73.95	125.36	0.1958	0.00676	0.02987
2489.	92.80	91.63	102.90	102.26	74.35	77.01	125.42	0.2176	0.00670	0.02940
2685.	91.37	90.45	101.62	101.10	72.89	76.62	125.17	0.2537	0.00640	0.02979
2976.	92.02	91.11	101.62	101.10	73.02	77.01	125.17	0.2989	0.00609	0.02793
3494.	90.85	90.06	100.58	99.81	70.62	73.15	124.86	0.3741	0.00595	0.02434
3772.	89.67	88.75	99.16	98.39	69.28	71.82	124.73	0.4224	0.00564	0.02340
4161.	88.10	87.57	98.13	97.61	67.53	70.48	125.54	0.5312	0.00538	0.02503
4946.	88.10	87.57	97.35	96.96	68.07	71.02	125.36	0.6371	0.00495	0.01902

VITA

John Louis Guillory

Candidate for the Degree of

Doctor of Philosophy

Thesis: DEHUMIDIFICATION OF AIR FLOWING BETWEEN PARALLEL PLATES

Major Field: Mechanical Engineering

Biographical:

Personal Data: Born in Lake Charles, Louisiana, January 8, 1940, the son of Mr. and Mrs. Clarence P. Guillory.

Education: Graduated from LaGrange Senior High School, Lake Charles, Louisiana, in May, 1957; received Bachelor of Science degree in Mechanical Engineering from the University of Southwestern Louisiana, Lafayette, Louisiana, in May, 1962; received Master of Science degree in Mechanical Engineering From Louisiana State University, Baton Rouge, Louisiana, in January, 1965; completed requirements for degree of Doctor of Philosophy at Oklahoma State University in May, 1973.

Professional Experience: Graduate teaching assistant, Mechanical Engineering Department, Louisiana State University, 1962-64; instructor, Department of Mechanical Engineering, University of Southwestern Louisiana, 1964-65; mechanical development engineer, Ethyl Corporation, 1965-66 and 1967-69; instructor, Mechanical Engineering Department, Louisiana State University, 1966-67: graduate teaching assistant, School of Mechanical and Aerospace Engineering, Oklahoma State University, 1969-71; assistant professor, California Polytechnic State University, 1971-72; pollution research engineer, John Zink Company, 1972 to present.

Professional Associations: American Society of Mechanical Engineers; Registered Professional Engineer (Louisiana).